ELSEVIER

Chemical Geology 209 (2004) 27–48

CHEMICAL GEOLOGY
INCLUDING
ISOTOPE GEOSCIENCE

www.elsevier.com/locate/chemgeo

Late Mesozoic volcanism in the northern Huaiyang tectono-magmatic belt, central China: partial melts from a lithospheric mantle with subducted continental crust relicts beneath the Dabie orogen?

Wei-Ming Fan[a,*], Feng Guo[a], Yue-Jun Wang[a], Ming Zhang[b]

[a] *Key Laboratory of Marginal Sea Geology, Guangzhou Institute of Geochemistry and South China Sea Institute of Oceanology, Chinese Academy of Sciences, Wushan, Guangzhou, 510640, PR China*

[b] *ARC National Key Center for Geochemical Evolution and Metallogeny of Continents (GEMOC), Department of Earth and Planetary Sciences, Macquarie University, NSW 2109, Australia*

Received 12 June 2003; accepted 9 April 2004

Abstract

Geochemistry of two groups of late Mesozoic volcanic rocks from the north Huaiyang belt (NHB) of the northern Dabie orogen provide evidence for their derivation from an enriched lithospheric mantle with subducted continental crustal relicts. The older group (149–137 Ma) consists of trachyandesites and trachydacites, showing light rare earth element (LREE) and large ion lithophile element (LILE) enrichment and strong high field strength element (HFSE, e.g., Nb, Ta, P and Ti) depletion, and highly enriched Sr–Nd isotopic signatures ($^{87}Sr/^{86}Sr(i) = 0.7082–0.7098$ and $\varepsilon_{Nd}(t) = -24.4$ to -19.1). Despite variations in SiO_2, MgO and isotopic ratios, they exhibit slight change in TiO_2, P_2O_5, Nb and LREE, suggesting that source differences rather than magmatic processes could be a major controlling factor for their genesis. The younger group (132–116 Ma) is mainly composed of basaltic trachyandesites and trachyandesites, having more significant LREE and LILE enrichment and HFSE depletion but less enriched Sr–Nd isotopic compositions ($^{87}Sr/^{86}Sr(i) = 0.7080–0.7084$ and $\varepsilon_{Nd}(t) = -19.2$ to -16.2) than the older group. The time-integrated elemental and isotopic variations from groups 1 to 2 show that less continental crustal materials were involved in producing the younger group of basaltic magmas because of easy exhaustion of the crustal rocks trapped in the lithospheric mantle during generation of the older intermediate-felsic melts. The petrogeneses of the two volcanic suites in the NHB imply that, though some of the subducted continental slices were rapidly exhumed to the crust shortly after collision, a significant volume of the subducted continental crust might be trapped in the lithospheric mantle.

Keywords: Late Mesozoic volcanic rocks; Geochemistry; Subduction; Continental crust; Subcontinental lithospheric mantle; Dabie orogen

1. Introduction

The discovery of high to ultrahigh-pressure (HP-UHP) minerals such as coesite and diamond inclu-

* Corresponding author. Tel.: +86-10-68597523; fax: +86-10-68597583.

E-mail address: wmfan@cashq.ac.cn (W.-M. Fan).

0009-2541/$ - see front matter © 2004 Elsevier B.V. All rights reserved.
doi:10.1016/j.chemgeo.2004.04.020

sions in eclogites from the Dabie-Sulu orogenic belt suggests that the continental crust was subducted to mantle depths during the Triassic (about 240 Ma) collision between the North China and Yangtze Blocks (e.g., Mattauer et al., 1985; Xu et al., 1992; Okay et al., 1993; Ernst and Liou, 1995; Cong, 1996; Li et al., 1993, 1999; Hacker et al., 1995, 1998; Zheng et al., 2002). The subducted slabs might have interacted with the surrounding mantle to form an enriched lithospheric mantle that served as a source component for early Cretaceous mafic to ultramafic intrusions and basaltic lavas (Jahn et al., 1999; Fan et al., 2001; Li et al., 1998) and even for the Cenozoic basalts in Hefei basin and its adjacent areas (Cong et al., 1996; Li et al., 1997). Following continental subduction and continent–continent collision, the HP-UHP metamorphic rocks were exhumed to crustal levels (e.g., Eide et al., 1994; Ames et al., 1993, 1996; Cong, 1996; Rowley et al., 1997; Jahn et al., 1999; Li, 1994; Li et al., 1993, 1999; Hacker et al., 1995). It is generally agreed that the subducted continental slice was rapidly exhumed to the middle crustal level at 226–214 Ma and to the surface starting from ~ 175 Ma as a result of slab breakoff (e.g., Li et al., 1999; Chen et al., 1995; Xu et al., 1999). The question remains whether subducted continental slabs can be trapped in the lithospheric mantle during continental subduction and subsequent exhumation.

Our investigations of late Mesozoic volcanics in the northern Huaiyang tectono-magmatic belt (NHB), a northern unit of the Dabie orogen, identified two volcanic sequences (the earlier volcanic suite termed as group 1 suite and the later as group 2 suite). Both exhibit time-integrated geochemical and isotopic variations that indicate that they were derived from heterogeneous sources as a mixture between a subducted continental middle-lower crust with geochemical affinity of the Yangtze Block and an enriched subcontinental lithospheric mantle formed during or shortly after the Triassic collision between the North China and Yangtze Blocks. In this paper, we present major and trace element and Sr–Nd isotopic data of the two groups of volcanic rocks in an attempt to address the following questions: (1) petrogenesis of the late Mesozoic volcanic rocks; (2) the role of deeply subducted continental crust as a source component for the late Mesozoic volcanism; and (3) mechanism and possible causes for preservation and digestion of the continental materials in the enriched lithospheric mantle after the collision.

2. Geological background

The various aspects of general geology of the Dabie orogenic belt have been widely discussed in the literature (e.g., Xu et al., 1992; Okay and Sengör, 1993; Cong, 1996; Jahn et al., 1999; Ames et al., 1996; Hacker et al., 1998). From south to north, the Dabie orogen comprises four litho-tectonic units: the Susong greenschist/blueschist belt (ST), the southern Dabie HP-UHP metamorphic complex (SDC), the northern Dabie orthogneiss complexes (NDC) and the NHB (Fig. 1). The NDC is mainly composed of gray gneisses of TTG compositions and subordinate migmatite, amphibolite, garnet granulite and marble, extensively intruded by the early Cretaceous granitic plutons and/or mafic–ultramafic intrusives (e.g., Jahn et al., 1999; Wang et al., 1996). It has long been debated about the tectonic affinity of the NDC metamorphic complexes. Wang et al. (1996) and Okay et al. (1993) interpreted it as thermally overprinted subduction/collision complexes, while Hacker et al. (1998) and Xue et al. (1997) regarded it as a Cretaceous extensional-magmatic complex. Other viewpoints such as a Paleozoic Andean-type magmatic arc complex (Wang et al., 1996), a metamorphic ophiolite mélange or hangingwall of the Sino-Korean Craton during Triassic subduction (Hacker et al., 2000) have also been postulated.

The NHB is located north of the Xiaotian-Mozitan detachment fault (Fig. 1). It is considered as a foreland basin of the Dabie orogenic belt, or as an important Mesozoic tectono-magmatic belt between the North China and Yangtze block. Its basement is mainly composed of low-grade metamorphic rocks with minor amphibolite-facies metamorphic rocks (e.g., Foziling and Luzhenguan Groups), which are commonly interpreted as flysch deposits or passive continental apron deposits of the Yangtze Block (e.g., Okay et al., 1993; Cong, 1996). During late Triassic to Jurassic, the NHB was a foreland basin of the Dabie Orogen, in which developed molasse deposits and medium to coarse-grained sandstones of thousands meters thick and compression-dominated structures (e.g., Hacker et al., 2000). Since late Mesozoic,

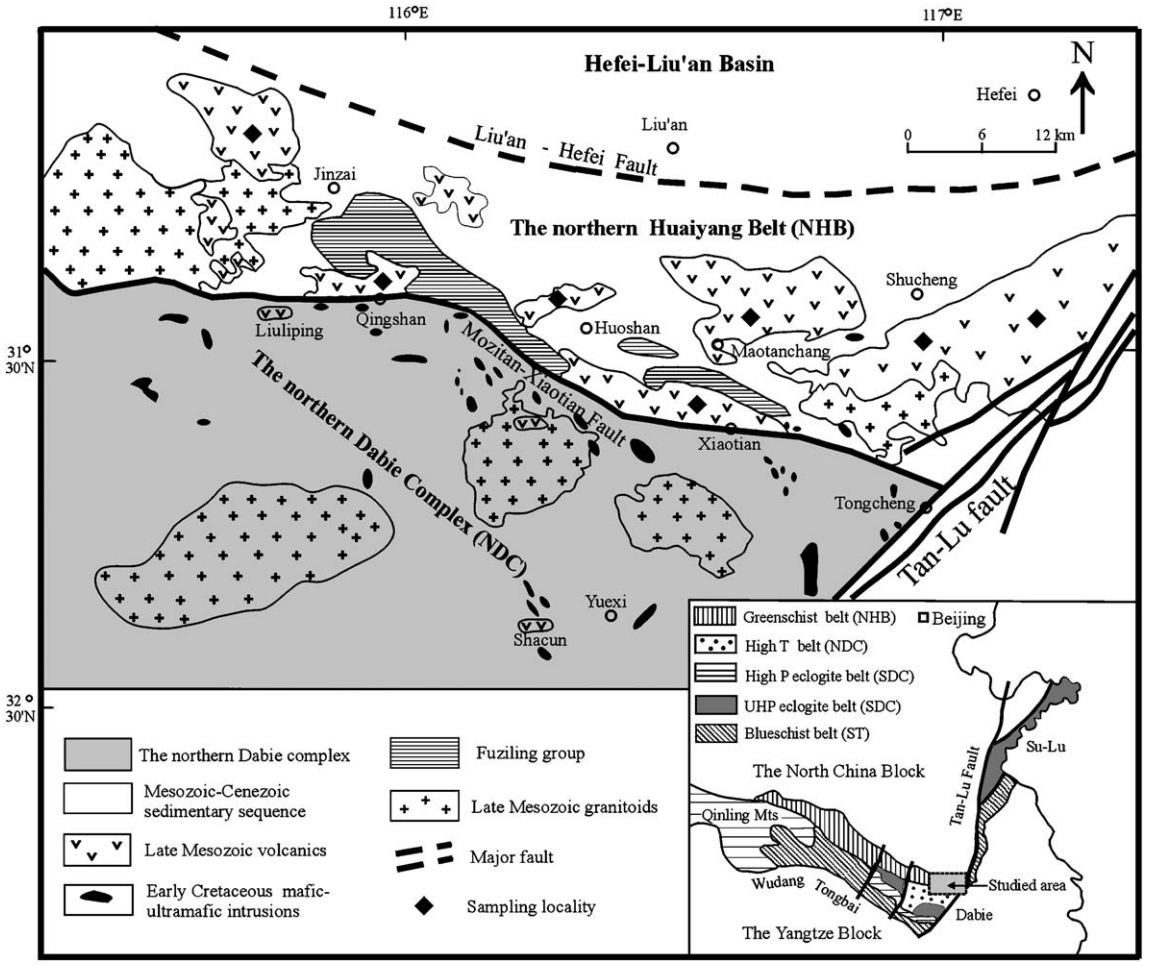

Fig. 1. A schematic geological map of the NHB in the Dabie orogen, showing the distribution of late Mesozoic volcanic rocks and the early Cretaceous mafic–ultramafic intrusions and the granitic plutons. The tectonic subdivision of the Dabie orogenic belt is modified after Jahn et al. (1999).

extensional and strike-slip structures are predominant (Ratschbacher et al., 2000), accompanied by eruption of voluminous volcanic sequences, emplacement of massive granitic plutons and scattered mafic–ultramafic intrusions and dykes (Ma et al., 1998; Jahn et al., 1999; Fig. 1).

These late Mesozoic volcanic rocks in the NHB constitute an EW-trending volcanic belt (Fig. 1). The volcanic sequences include Maotanchang Fm., Xiaotian Fm. and Jingangtai Fm. They mainly consist of basaltic trachyandesite, trachyandesite, trachyte lava flows, tuff and volcanic breccia. From field investigations, the volcanic sequences truncate the Proterozoic metamorphic volcano-sedimentary series and overlie middle to Upper Jurassic molasses deposits, underlain conformably or pseudo-conformably by Upper Cretaceous Heishidu Fm. (e.g., Wang et al., 2002). These volcanics can be temporarily and lithologically divided into two groups (1 and 2), separated by a conglomerate layer that consists of polygenic gravels, including granites, gneisses and volcanics. The older group (group 1) lavas erupted from 149 to 137 Ma (Wang et al., 2002) and the younger group (group 2) rocks erupted from 132 to 116 Ma (Yang et al., 1999; Zhou et al., 1995; Wang et al., 2002). Lithologically, the group 1 rocks are mainly com-

Table 1
Major and trace element contents of the late Mesozoic group 1 volcanic rocks in the NHB

Sample	99SC-4	99SC-5	99SC-7	99SC-9	99SC-10	99SC-12	99SC-14	99SC-11	99MTC-16	99MTC-17	99XT-6	99MTC-19	99MTC-24	99MTC-27
Rock type	T	TA	TA	TA	TA	TA	TA	TA	T	T	TA	TA	TA	TA
SiO_2	65.64	57.85	58.00	60.10	59.69	59.49	59.98	60.07	63.18	61.11	67.08	62.28	63.39	63.11
Al_2O_3	14.42	14.63	15.08	15.02	14.85	15.09	14.91	15.12	16.22	17.04	13.92	13.76	16.63	16.67
Fe_2O_3	6.08	5.14	4.42	5.23	5.43	5.68	4.56	5.64	2.62	4.43	3.41	3.97	4.07	4.82
FeO	0.15	1.36	1.87	1.33	1.33	1.24	1.99	1.06	1.65	1.42	1.12	0.13	0.28	1.09
CaO	0.75	2.62	2.94	4.75	4.80	4.77	3.47	4.04	2.71	2.91	2.66	6.65	3.96	2.18
MgO	0.56	4.12	3.79	3.76	3.77	3.81	4.32	3.59	1.84	1.24	1.85	0.94	1.25	1.28
Na_2O	2.71	2.41	2.83	3.89	4.04	4.02	4.11	3.85	4.72	7.05	3.54	4.07	4.13	4.40
K_2O	7.28	7.01	6.34	3.36	3.40	3.37	3.52	3.84	4.04	2.34	3.94	3.46	3.92	3.96
MnO	0.02	0.11	0.10	0.08	0.08	0.08	0.06	0.08	0.10	0.09	0.05	0.14	0.08	0.05
TiO_2	0.74	0.82	0.82	0.81	0.80	0.82	0.80	0.80	0.64	0.88	0.64	0.53	0.65	0.85
P_2O_5	0.26	0.27	0.28	0.27	0.27	0.27	0.27	0.27	0.24	0.33	0.20	0.23	0.27	0.31
LOI	0.90	3.01	2.98	1.07	1.19	1.02	1.61	1.28	1.70	0.90	1.24	3.57	1.03	0.93
Total	99.51	99.35	99.45	99.67	99.65	99.66	99.60	99.64	99.66	99.74	99.65	99.73	99.66	99.65
Mg#	0.17	0.58	0.57	0.56	0.55	0.55	0.59	0.50	0.49	0.32	0.47	0.34	0.39	0.32
V	83	108	160	106	88	93	129	67	69	109	69	37	72	104
Cr	85	101	93	95	104	92	96	42	7	11	28	23	22	14
Ni	19	34	33	71	38	33	36	20	8	13	15	9	10	11
Rb	231	208	182	73.2	73.4	64.3	74.8	105	68	50.2	67.9	62.3	80.4	89.7
Sr	367	503	408	700	732	662	788	746	478	446	558	507	523	620
Ba	2366	2969	2718	2432	2435	2333	1469	2049	1891	990	1806	2943	2581	1779
Th	7.32	7.13	7.33	7.28	7.33	7.53	7.32	9.21	7.94	6.86	6.31	7.11	8.12	8.07
Zr	207	171	150	163	145	143	253	336	210	286	153	306	357	294
Hf	5.80	4.99	4.60	5.13	4.40	4.12	6.52	8.29	5.57	6.85	4.22	7.12	8.19	6.97
Nb	11.2	12.1	11.8	12	12.4	11.7	12.1	12.2	10	9.9	9.4	11.7	13.5	12.4
Ta	0.68	0.89	0.69	0.66	0.73	0.68	1.98	0.76	0.64	0.59	0.53	0.63	0.74	0.75
Y	18.15	23.83	24.24	25.18	25.40	23.81	23.66	20.89	13.18	17.48	16.21	22.46	24.16	21.77
La	52.13	50.31	50.04	51.35	50.06	48.20	56.56	56.56	49.23	51.10	42.56	47.17	50.76	50.40
Ce	99.42	98.13	99.24	100.0	100.1	95.36	92.09	92.09	95.68	101.5	79.0	92.0	101.3	94.19
Pr	10.36	10.98	10.85	10.79	10.86	10.27	10.40	10.40	10.14	10.53	8.44	8.96	10.51	10.43
Nd	32.28	40.31	39.91	40.21	40.38	39.38	36.40	36.40	34.11	37.10	29.43	31.87	36.66	38.80
Sm	7.22	8.40	7.99	8.00	7.97	8.11	6.93	6.93	6.64	7.59	5.57	6.26	8.13	7.51
Eu	1.42	1.87	1.84	1.72	1.72	1.82	1.52	1.52	1.34	1.79	1.38	1.41	1.57	1.89
Gd	5.03	6.23	6.41	6.43	6.64	5.88	5.14	5.14	4.10	5.42	4.21	5.04	5.76	5.83
Tb	0.70	0.85	0.90	0.91	0.90	0.81	0.68	0.68	0.55	0.66	0.62	0.76	0.82	0.82
Dy	3.93	5.14	5.27	5.19	5.35	5.03	4.12	4.12	2.87	3.62	3.32	4.61	4.81	4.39
Ho	0.76	0.94	0.94	0.96	1.00	0.93	0.80	0.80	0.48	0.72	0.62	0.84	0.87	0.85
Er	2.05	2.62	2.69	2.88	2.95	2.51	2.19	2.19	1.39	1.80	1.65	2.43	2.74	2.18
Tm	0.27	0.36	0.32	0.39	0.37	0.37	0.38	0.38	0.16	0.26	0.24	0.35	0.39	0.33
Yb	1.79	2.21	2.34	2.37	2.42	2.35	2.12	2.12	1.19	1.61	1.34	2.54	2.46	2.07
Lu	0.30	0.37	0.33	0.37	0.36	0.36	0.31	0.31	0.18	0.23	0.22	0.39	0.38	0.30

Sample	99MTC-34	99MTC-37	99MTC-41	99MTC-42	99MTC-44	99XHL-1	99XHL-2	99XHL-4	99XHL-5	99XHL-7	99JZ-16	99XT-7	99SC-15
Rock type	TA	TA	TA	TA	T	TA	TA	TA	TA	TA	TA	T	T
SiO_2	60.52	61.87	58.88	59.62	61.33	57.64	56.89	57.50	55.29	60.96	60.53	63.44	63.52
Al_2O_3	17.61	16.47	17.12	17.75	15.98	15.65	15.55	15.77	15.42	14.89	15.28	14.96	16.42
Fe_2O_3	4.78	4.89	5.32	5.64	6.74	2.78	2.93	3.08	2.93	3.95	2.12	4.13	4.44
FeO	0.30	0.57	1.00	0.49	0.52	2.92	2.86	3.04	2.95	0.97	3.49	1.51	0.13
CaO	2.72	3.78	4.39	3.05	3.31	5.25	5.42	5.42	5.53	3.67	2.99	3.15	1.02
MgO	1.30	1.63	2.46	1.36	1.58	1.85	2.16	1.84	2.15	1.65	2.69	2.43	2.06
Na_2O	5.55	5.74	5.83	6.06	5.94	3.47	3.29	3.34	3.30	2.36	3.46	4.42	4.83
K_2O	4.71	2.46	2.59	3.26	1.85	2.97	2.98	2.89	2.81	3.26	3.55	3.25	5.06
MnO	0.06	0.05	0.06	0.03	0.04	0.12	0.11	0.10	0.13	0.08	0.10	0.06	0.05
TiO_2	0.68	0.87	0.79	0.81	0.95	0.69	0.73	0.73	0.72	0.62	0.74	0.68	0.56
P_2O_5	0.30	0.32	0.27	0.33	0.37	0.29	0.29	0.30	0.30	0.25	0.25	0.22	0.22
LOI	1.11	1.01	0.97	1.16	1.12	6.03	6.45	5.62	8.18	7.04	4.41	1.37	1.22
Total	99.64	99.66	99.68	99.56	99.73	99.66	99.66	99.63	99.71	99.70	99.61	99.62	99.53
Mg#	0.36	0.40	0.46	0.33	0.32	0.42	0.45	0.40	0.45	0.42	0.51	0.49	0.47
V	84	114	123	101	141	94	102	104	105	79	116	104	67
Cr	28	30	81	11	20	11	11	11	10	28	28	32	42
Ni	11	15	27	8	12	8	8	9	8	18	13	15	20
Rb	90.1	51.2	56.0	69	44.8	71	76.8	73.3	75.6	75.1	168	60.1	105
Sr	567	658	686	796	675	600	572	626	625	521	377	630	746
Ba	3261	1430	1527	2233	2040	1578	1558	1592	1260	1498	1738	1720	2049
Th	6.91	6.91	6.07	5.85	5.22	11.66	11.91	11.90	11.90	8.01	11.32	6.73	9.21
Zr	380	278	244	314	289	192	214	221	192	72	214	162	336.1
Hf	9.12	6.71	6.35	7.65	6.44	4.88	4.98	5.33	5.07	2.16	5.68	4.11	8.29
Nb	14	9.7	9.1	12.1	11.5	11.3	11.4	11.6	11.7	8.5	10	10.5	12.2
Ta	0.81	0.55	0.52	0.66	0.63	0.71	0.70	0.75	0.77	0.56	0.70	0.61	0.76
Y	23.20	17.70	16.21	20.30	23.21	19.24	19.28	19.37	19.93	14.22	21.98	19.09	20.89
La	50.06	58.35	41.41	51.69	49.59	54.80	55.44	57.15	56.82	45.95	46.30	44.40	56.56
Ce	96.82	100.7	84.06	101.7	97.85	100.8	103.4	105.4	104.3	86.45	88.22	82.39	92.09
Pr	10.37	11.43	9.49	11.24	10.68	10.60	10.59	10.90	10.69	9.18	9.29	8.68	10.40
Nd	37.35	38.31	33.09	39.27	39.47	34.55	37.64	36.52	36.97	31.49	33.23	31.32	36.40
Sm	7.11	7.36	6.59	7.90	8.46	6.73	6.81	6.47	6.65	5.81	7.02	6.30	6.93
Eu	1.55	1.74	1.52	1.57	1.91	1.51	1.65	1.59	1.68	1.42	1.41	1.50	1.52
Gd	5.49	4.91	4.78	5.34	6.17	4.82	5.00	4.96	5.01	4.30	5.31	4.78	5.14
Tb	0.80	0.65	0.58	0.78	0.86	0.63	0.70	0.68	0.68	0.56	0.73	0.68	0.68
Dy	4.77	3.44	3.66	4.35	4.88	3.64	3.86	3.86	3.97	2.96	4.36	3.83	4.12
Ho	0.95	0.64	0.63	0.81	0.92	0.73	0.74	0.76	0.72	0.53	0.81	0.75	0.80
Er	2.66	1.91	1.79	2.22	2.51	2.12	2.10	2.21	2.21	1.55	2.47	2.04	2.19
Tm	0.40	0.23	0.23	0.29	0.34	0.28	0.29	0.28	0.31	0.20	0.35	0.28	0.38
Yb	2.73	1.67	1.68	2.05	2.27	2.03	2.15	2.21	2.09	1.30	2.42	1.88	2.12
Lu	0.39	0.22	0.24	0.32	0.31	0.28	0.31	0.33	0.35	0.17	0.33	0.27	0.31

BT = basaltic trachyandesites, TA = trachyandesites, T = trachyte, LOI = loss of ignition.

posed of trachyandesites and trachytes, while the group 2 rocks comprise mainly basaltic trachyandesites and trachyandesites.

Trachyandesites from group 1 are subprophyric with predominant phenocrysts of hornblende (2–4 mm) and plagioclase (2–5 mm), and minor K-feldspar (1–3 mm) and quartz (~ 1 mm). The groundmass consists of fine-grained (0.2–0.5 mm) amphibole and feldspar and glass, and a few opaque oxides. Mafic inclusions, xenocrysts and amygdaloid were rarely found in these rocks. Most samples are fresh and free of surface alteration except for those (99XHL-1–7) from Xianhualing that experienced strong chloritization and carbonatization as reflected by the high LOI (the maximum is up to 8%) (Table 1). The trachytes are massive lavas with aphyric to aphanitic fabric, containing phenocrysts of K-feldspar (1–3 mm) and quartz (~ 1 mm) set in a matrix of predominant glass and minor fine-grained feldspar, quartz and opaque oxides. These samples are fairly fresh and a few of them experienced weak kaolinization. Most basaltic trachyandesites and trachyandesites in group 2 are fresh, and some of them underwent weak chloritization. They exhibit weakly porphyritic fabric rather rich in hornblende (1–2 mm) and clinopyroxene (2–3 mm) phenocrysts that set in a matrix of fine-grained feldspar, clinopyroxene and hornblende and minor opaque oxides.

3. Analytical techniques

All samples were crushed to mm scale after removal of weathered rims and handpicked under a binocular microscope. Only fresh chips were selected and cleaned in an ultrasonic bath with de-ionised water. These chips were then crushed to <20 mesh in a WC jaw crusher. A split was ground to <160 mesh grain size in an agate ring mill for major and trace element analysis. Major elements were analyzed at Hubei Institute of Geology and Mineral Resource, Ministry of Land and Resources (MLR), by wavelength X-ray fluorescence spectrometry (XRF) with analytical errors ≤2%. FeO content was analyzed by a wet chemical method. The repetitive analytical results of international standard samples of GSR-1 (granite), GSR-2 (andesite) and GSR-3 (basalt) are listed in Appendix A.

Trace element abundances of the samples were determined using an inductively coupled plasma mass spectrometer (ICP-MS) at Guiyang Institute of Geochemistry, Chinese Academy of Sciences (CAS). The powders of about 100 mg were placed in a screw-top PTFE-lined stainless steel bomb and dissolved by HF and HNO3. The sealed bombs were placed in an electric oven and heated to 190 °C for 12 h. Before ICP-MS performance, 1 ppm Rh solution was added as an internal standard. The analytical errors are estimated to be less than 5% for elements >10 ppm and about 10% for transition metals such as Cr, Ni, V and Sc from repetitive analyses of international standards of BHVO-1 (basalt) and AMH-1 (andesite). Duplicate runs gave <10% RSD (relative standard deviation) for most analyzed elements except for transition metals that generally gave <20% RSD. Detailed description of the analytical technique was reported by Qi et al. (2000).

Sr and Nd isotopic ratios were performed at the Institute of Geology and Geophysics, CAS. The rock chips crushed to <20 meshes were leached by purified 6N HCl for 24 h at room temperature before dissolution to remove altered and weathered surfaces of the samples. The Sr and Nd isotopic ratios were normalized to $^{86}Sr/^{88}Sr = 0.1194$ and $^{146}Nd/^{144}Nd = 0.7219$, respectively. Thirteen analyses of the standard La Jolla give $^{143}Nd/^{144}Nd = 0.511862 \pm 10$ and two analyses of BCR-1 give $^{143}Nd/^{144}Nd = 0.512626 \pm 9$. Six analyses of NBS 987 yield $^{87}Sr/^{86}Sr = 0.710265 \pm 12$ and $^{87}Sr/^{86}Sr = 1.20032 \pm 3$ for two analyses of NBS607. Total procedure blanks are about $2–5 \times 10^{-10}$ g for Sr and less than 5×10^{-11} g for Nd. $^{87}Rb/^{86}Sr$ and $^{147}Sm/^{144}Nd$ ratios were calculated using the Rb, Sr, Sm and Nd concentrations by ICP-MS analyses. $^{87}Sr/^{86}Sr(i)$ and $\varepsilon_{Nd}(t)$ were calculated using K–Ar age of 140 Ma for group 1 and 130 Ma for group 2, respectively (Wang et al., 2002). Major and trace elemental abundances and Sr–Nd isotopic ratios of the samples are listed in Tables 1–3 .

4. Results

4.1. Major elements

All major element contents are normalized to 100% on LOI (loss of ignition)-free basis before plotted in

Table 2
Major and trace element contents of the late Mesozoic group 2 volcanic rocks in the NHB

Sample	99XT-1	99XT-2	99XT-3	99XT-4	99XT-11	99XT-15	20BHY-7	20BHY-8	20BHY-9	20BHY-11	20BHY-13	20BHY-14	20BHY-15	20BHY-16	20BHY-17	20BHY-19
Rock type	TA	TA	TA	TA	TA	TA	TA	TA	TA	TA	BT	BT	TA	TA	TA	TA
SiO_2	55.24	54.91	55.10	55.31	56.39	57.22	55.2	55.06	56.01	53.81	51.73	51.21	54.97	56.20	56.80	56.40
Al_2O_3	15.30	15.60	15.66	15.06	15.07	14.74	15.15	15.39	15.2	16.23	15.42	15.52	15.71	15.05	15.1	14.90
Fe_2O_3	2.85	3.11	2.92	3.56	3.54	4.00	3.67	3.34	2.82	2.80	3.91	5.56	3.27	3.25	4.10	4.16
FeO	4.00	4.18	3.85	3.61	3.12	3.19	3.75	3.75	4.37	4.17	4.03	2.93	3.98	4.23	2.93	3.40
CaO	5.89	5.39	4.79	5.12	5.33	4.24	4.85	5.13	5.69	5.89	6.34	5.19	4.94	4.51	4.29	4.23
MgO	3.87	4.03	4.36	4.01	2.41	4.04	4.57	4.51	3.19	5.17	6.62	6.05	4.52	4.29	3.99	4.48
Na_2O	2.86	3.17	4.65	4.61	4.86	3.75	4.37	3.70	3.60	2.98	3.10	3.67	4.31	3.89	3.85	3.61
K_2O	4.70	4.42	3.87	3.19	3.32	3.98	3.29	3.98	3.97	4.23	3.06	3.24	3.49	3.58	4.19	3.84
MnO	0.15	0.13	0.10	0.09	0.10	0.06	0.10	0.11	0.14	0.13	0.11	0.10	0.10	0.10	0.07	0.07
TiO_2	1.30	1.34	1.34	1.30	1.28	1.30	1.28	1.31	1.3	1.28	1.55	1.56	1.36	1.33	1.29	1.32
P_2O_5	0.71	0.71	0.73	0.73	0.72	0.77	0.74	0.72	0.71	0.79	0.85	0.85	0.70	0.71	0.80	0.73
LOI	2.55	2.41	2.10	2.99	3.41	2.21	2.58	2.50	2.49	1.65	2.87	3.49	2.19	2.34	2.12	2.33
Total	99.42	99.40	99.47	99.58	99.55	99.50	99.55	99.50	99.49	99.13	99.59	99.57	99.54	99.48	99.53	99.47
Mg#	0.55	0.55	0.59	0.55	0.44	0.55	0.58	0.58	0.49	0.54	0.65	0.61	0.58	0.56	0.56	0.57
V	135	138	134	128	131	134	125	138	136	143	161	155	134	128	131	121
Cr	158	157	159	166	157	91.9	170	169	169	154	208	204	112	123	97.1	90.2
Ni	66.0	62.2	61.5	65.0	64.5	38.8	69.1	68.9	70.2	68.7	83.5	81.5	46.9	55.4	48.6	35.4
Rb	117.5	89.4	87.2	75.3	65.4	102.7	84.1	105.2	105.9	198.1	78.3	78.9	94.2	87.7	115.7	97.4
Sr	1228	974	1052	980	783	1002	829	1405	1350	1219	1009	955	1247	1077	1055	920
Ba	2591	2877	2198	1736	1804	1965	1888	2210	2188	3818	1970	1980	2107	2555	2217	2227
Th	10.44	10.76	10.92	11.26	10.87	11.14	11.17	10.76	10.80	11.80	7.96	7.91	11.15	11.14	11.61	10.73
Zr	403	413	413	415	393	404	377	377	374	421	339	327	371	376	383	346
Hf	8.89	8.99	9.18	9.06	8.44	8.78	10.61	9.83	9.81	12.26	8.96	8.30	9.53	10.22	10.23	9.40
Nb	20.32	20.25	20.06	20.53	19.39	21.75	20.90	20.85	20.33	26.91	26.21	24.81	22.89	21.89	22.13	20.51
Ta	0.93	0.95	1.01	0.99	0.95	1.08	1.00	1.02	0.97	1.30	1.24	1.26	1.09	1.04	1.07	0.94
Y	26.23	25.88	26.61	26.67	24.93	25.03	27.67	27.67	27.25	31.93	26.78	25.44	27.42	26.45	26.98	24.50
La	92.01	93.04	94.37	96.38	93.11	97.80	100.5	97.84	97.15	97.47	87.36	87.63	98.79	102.7	103.8	94.07
Ce	178.5	180.7	181.7	186.6	179.5	188.7	192.7	189.3	188.6	190.7	175.6	172.1	190.1	195.6	197.8	183.1
Pr	19.00	19.48	19.20	20.02	18.84	19.59	20.49	20.11	19.93	20.36	18.98	18.77	20.02	20.71	20.61	19.22
Nd	69.55	71.36	71.93	72.63	67.72	70.77	75.16	76.02	75.25	76.01	73.22	70.34	75.22	76.48	76.80	71.32
Sm	12.63	12.60	12.69	12.92	12.36	12.28	14.06	12.24	12.67	13.43	12.34	12.49	12.30	12.27	12.37	11.56
Eu	2.65	2.64	2.49	2.63	2.52	2.38	3.18	3.06	3.05	3.44	3.09	3.09	3.03	2.80	2.85	2.72
Gd	8.27	8.83	8.44	8.67	8.19	8.26	8.39	8.33	8.19	9.17	8.38	7.84	7.88	8.02	7.76	7.49
Tb	1.08	1.11	1.10	1.12	1.07	1.04	1.19	1.19	1.12	1.25	1.20	1.16	1.11	1.13	1.09	1.07
Dy	5.84	5.67	5.80	6.05	5.87	5.56	6.13	5.84	5.97	6.84	5.69	5.66	5.76	5.22	5.46	5.09
Ho	0.94	1.01	1.03	1.03	1.00	0.95	1.03	1.02	1.05	1.25	1.03	1.03	0.97	1.02	1.02	0.94
Er	2.44	2.66	2.80	2.74	2.68	2.51	2.95	2.60	2.65	3.17	2.58	2.52	2.72	2.54	2.62	2.35
Tm	0.35	0.35	0.39	0.38	0.35	0.33	0.38	0.37	0.37	0.41	0.35	0.35	0.34	0.37	0.36	0.32
Yb	2.08	2.32	2.26	2.22	2.30	2.14	2.41	2.40	2.22	2.79	2.26	2.10	2.26	2.24	2.08	2.09
Lu	0.28	0.32	0.33	0.34	0.36	0.28	0.33	0.31	0.32	0.40	0.27	0.24	0.33	0.29	0.27	0.25

the SiO_2 vs. major and trace element diagrams (Figs. 2 and 3). The late Mesozoic volcanic rocks in the NHB span a large SiO_2 range of 53.3–68.2% and MgO range of 0.6–6.8%. The group 1 rocks have 59.7–68.2% SiO_2 and 0.6–4.4% MgO, whereas the group 2 rocks have 53.3–58.8% SiO_2 and 2.5–6.8% MgO. Both groups show high-K calc-alkaline to shoshonitic characteristics with high K_2O contents (generally K_2O>3.0%) (Tables 1 and 2 and Fig. 2a). In the TAS diagram (Fig. 2b), the group 1 rocks are mainly composed of trachydacites and trachyandesites, whereas the group 2 rocks are dominated by basaltic trachyandesites and trachyandesites (Middlemost, 1994). As illustrated in Fig. 2c, the group 1 lavas show a large variation in aluminum saturation index (A/CNK = Al_2O_3/(CaO + Na_2O + K_2O) in molecular ratio, 0.61–1.08), with metaluminous to slightly peraluminous characters, while the group 2 rocks show a narrow range of A/CNK ratios (0.71–0.84) with metaluminous affinity (Maniar and Piccoli, 1989).

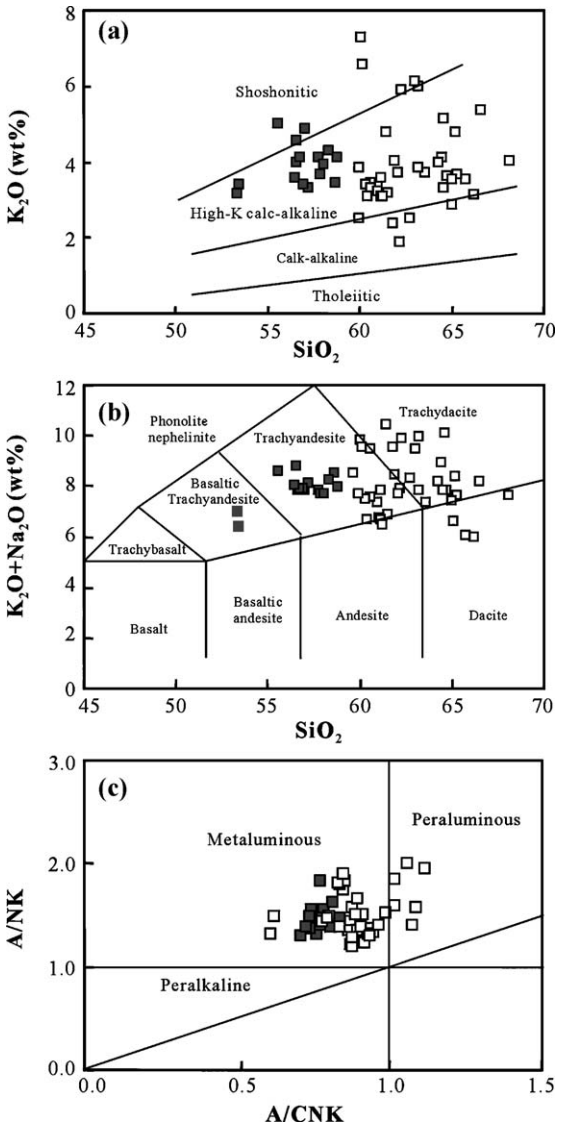

Fig. 2. SiO_2 vs. K_2O (a) and $K_2O + Na_2O$ (b) and A/NCK vs. A/NK (c) diagrams of late Mesozoic volcanic rocks in the NHB. Open and filled squares represent groups 1 and 2 rocks, respectively.

The mg-numbers (Mg# = 100 × Mg/(Mg + ΣFe) in atomic ratio) of the samples span a range from 65 to 30. Both groups of rocks show general negative correlations between FeO_T (FeO + Fe_2O_3), MgO and CaO and SiO_2, with slightly varied TiO_2 and P_2O_5 (Fig. 3). The group 2 rocks have higher TiO_2 and P_2O_5 with a limited range of K_2O/TiO_2 and K_2O/P_2O_5 ratios (2.0–3.6 and 3.6–6.6, respectively), while lower TiO_2 and P_2O_5 but larger variations of K_2O/TiO_2 and K_2O/P_2O_5 ratios (2.7–9.8 and 7.1–28, respectively) in the group 1 lavas.

4.2. Trace elements

Group 1: The group 1 lavas generally show slight variation in La, Nb and Sr, but random variation in Sr and Th over the range of SiO_2 (Fig. 3). Some samples containing higher proportion of hornblende phenocrysts (e.g., samples from Shucheng 99SC-5, 7, 9 and 10) generally have higher compatible element (e.g., Cr and Ni) concentrations (Table 1 and Fig. 5). In the chondrite-normalized rare earth element (REE) patterns, the group 1 lavas show strong light rare earth element (LREE) enrichment with high $(La/Yb)_{CN}$ ratios (14.7–25.3) and weak negative Eu anomalies (Eu*/Eu = 0.67–0.86). Heavy rare earth element (HREE) fractionation is weak with a (Gd/Yb)CN range of 1.66–2.73 (Fig. 4a). Their primitive mantle-normalized incompatible element spidergrams were characterized by strong LREE, large ion lithophile element (LILE) and K enrichment but Nb, Ta, Ti and P

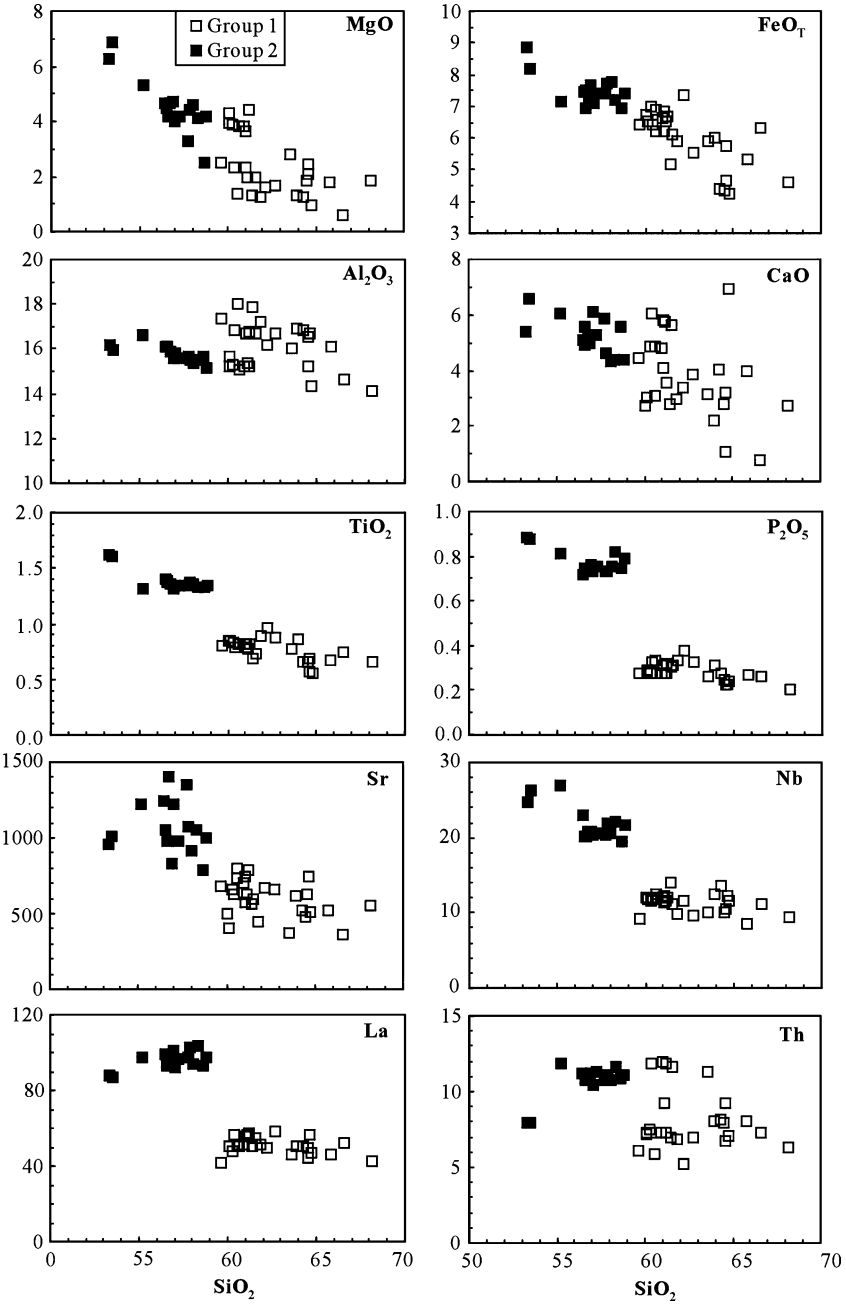

Fig. 3. Variations of major oxides and trace elements vs. SiO_2 of the late Mesozoic volcanic suites in NHB. Symbols as in Fig. 2.

depletion (Fig. 4c). Despite the large variations in Mg#, SiO_2 and Th that generally as differentiation indexes, Ni concentration in these rocks show random shift, possibly suggesting a less important role of fractional crystallization (FC) during magma evolution (Fig. 5).

Group 2: Compared to the group 1 lavas, the group 2 rocks generally show higher abundances in com-

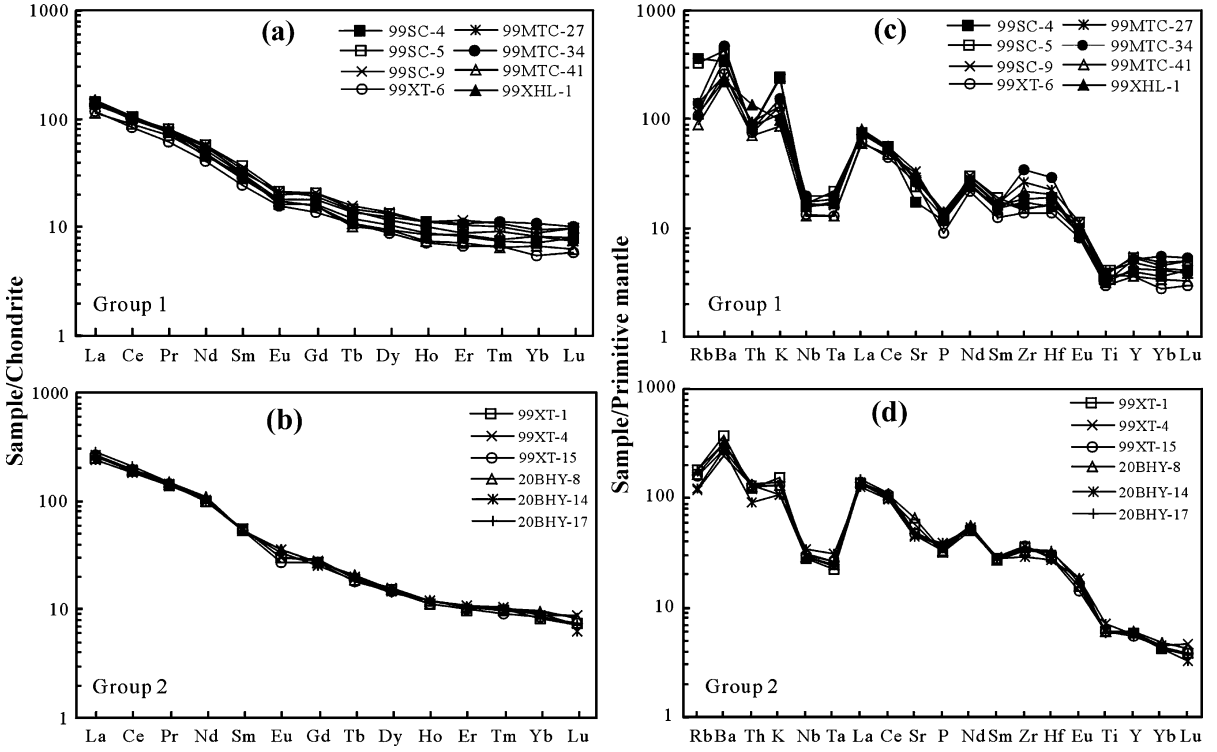

Fig. 4. Chondrite-normalized REE patterns (a and b) and primitive mantle-normalized incompatible element spidergrams (c and d) for representative samples of the late Mesozoic volcanic rocks in NHB. Note that all of the samples show LREE and LILE enrichment and Nb and Ta depletion. Data of primitive mantle are from Sun and McDonough (1989) and of chondrite are from Taylor and McLennan (1985).

patible elements such as Cr and Ni, and LREE and HFSE (Table 2, Figs. 3, 4b,d and 5). They also show steeper chondrite-normalized REE patterns, spanning a (La/Yb)CN range of 28–36 and a (Gd/Yb)CN range of 2.9–3.3 with weakly negative Eu anomalies (Eu*/Eu = 0.68–0.90) (Fig. 4b). Similar to the group 1 lavas, these rocks also display intensive LILE, LREE enrichment and Nb–Ta depletion in the primitive mantle-normalized spidergrams (Fig. 4d).

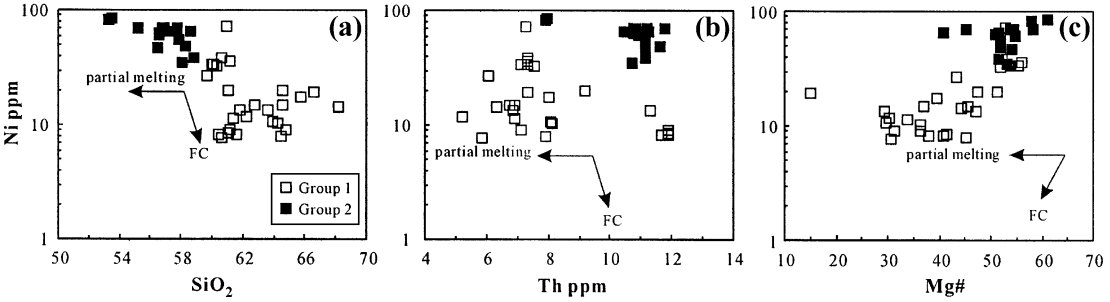

Fig. 5. Ni vs. SiO_2, Th and Mg# plots of late Mesozoic volcanic rocks in the NHB of Dabie orogen, showing possible magmatic processes during magma genesis. Symbols as shown in the figure.

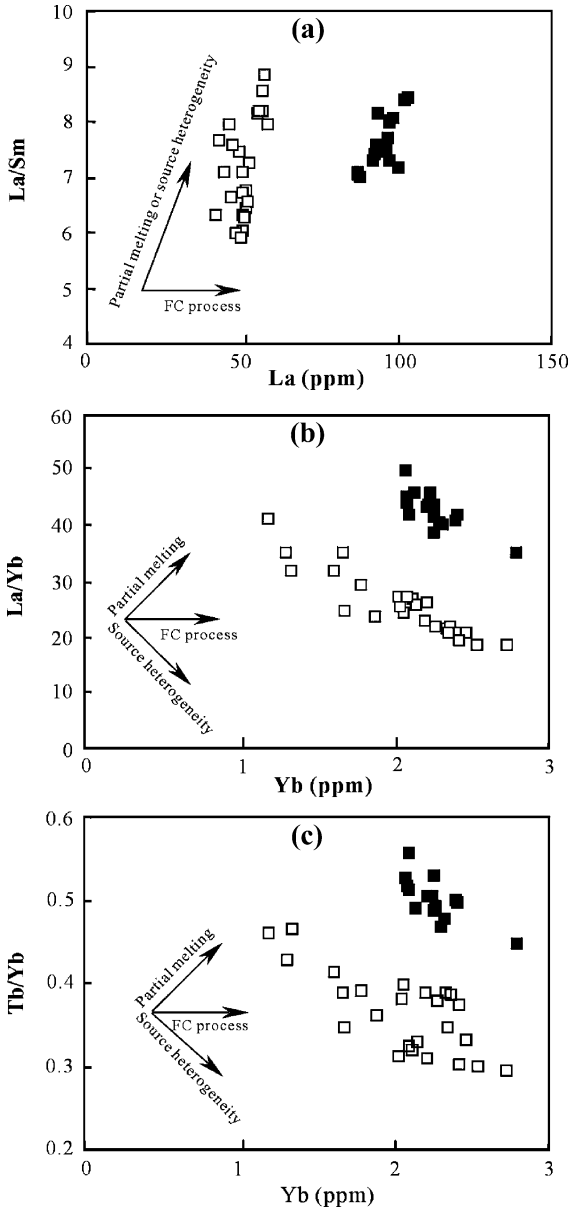

Fig. 6. La vs. La/Sm (a), Yb vs. La/Yb (b) and Yb vs. Tb/Yb (c) diagrams of the late Mesozoic volcanic rocks in the NHB. (a) The positive correlations of La/Sm vs. La indicate a less important role for FC than partial melting in the genesis of both groups. In (b) and (c), the negative trends between Yb and La/Yb, and Tb/Yb suggest that neither partial melting nor FC processes could be a major controlling factor to account for the unique geochemical feature in both volcanic suites, and possibly as a result of source heterogeneity. Symbols as in Fig. 2.

In the La vs. La/Sm, Yb vs. La/Yb and Yb vs. Tb/Yb diagrams (Fig. 6a–c), both groups exhibit a positive relationship between La and La/Sm but negative correlations between La/Yb and Yb, and Tb/Yb vs. Yb. Again, both groups have much higher Ba/Nb and La/Nb ratios than those of depleted mantle-derived melts such as MORB and OIB (e.g., Sun and McDonough), plotted within the variation range of arc volcanics in a Ba/Nb vs. La/Nb diagram (Fig. 7), as that defined by the early Cretaceous mafic–ultramafic intrusions in the NDC (Jahn et al., 1999).

4.3. Sr–Nd isotopes

Sr and Nd isotope data for 17 samples of group 1 and 8 samples of group 2 (Table 3) generally show a large range of $\varepsilon_{Nd}(t)$ value (−16.2 to −24.2) but a limited range of $^{87}Sr/^{86}Sr(i)$ ratios (0.7074–0.7098), overlapping the range of the early Cretaceous mafic–ultramafic intrusions in the NDC (Jahn et al., 1999), and gray gneisses in the northern Dabie complexes (Zheng et al., 2000; Ma et al., 2000) (Fig. 8). Compared to the group 2

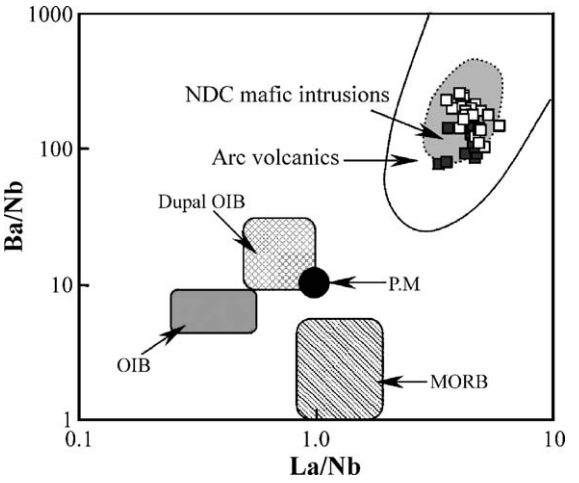

Fig. 7. La/Nb vs. Ba/Nb plots showing that the late Mesozoic volcanic rocks in the NHB have very high Ba/Nb and La/Nb ratios, similar to the early Cretaceous mafic–ultramafic intrusions in Dabie orogenic belt. Data sources: Arc volcanics and the early Cretaceous maficultramafic intrusions (Jahn et al., 1999); PM, OIB, MORB and Dupal OIB (Sun and McDonough, 1989). Symbols as in Fig. 2.

Table 3
Sr and Nd isotopic compositions of the late Mesozoic volcanic rocks in the NHB

Group	Sample	Nd (ppm)	Sm (ppm)	$^{147}Sm/^{144}Nd$	$^{143}Nd/^{144}Nd \pm 2$	Rb (ppm)	Sr (ppm)	$^{87}Rb/^{86}Sr$	$^{87}Sr/^{86}Sr \pm 2$	$^{87}Sr/^{86}Sr$ (i)	ε_{Nd} (t)
Group 1	99SC-4	32.28	7.22	0.11722	0.511447 ± 9	231.2	367	1.8287	0.711861 ± 12	0.70822	− 21.8
	99SC-5	40.31	8.40	0.12610	0.511467 ± 10	208.0	503	1.1992	0.711358 ± 12	0.70897	− 21.6
	99SC-9	40.21	8.00	0.12033	0.511453 ± 7	73.4	700	0.3039	0.709467 ± 32	0.70886	− 21.8
	99SC-12	39.38	8.11	0.11948	0.511459 ± 9	64.3	662	0.2817	0.709629 ± 20	0.70907	− 21.6
	99MTC-16	34.11	6.64	0.11775	0.511363 ± 7	64.8	478	0.3930	0.709184 ± 12	0.70842	− 23.6
	99XT-6	29.43	5.57	0.11441	0.511323 ± 11	67.9	558	0.3527	0.710429 ± 13	0.70978	− 24.4
	99MTC-24	36.66	8.13	0.13406	0.511431 ± 7	80.4	507	0.4458	0.710017 ± 15	0.70910	− 22.4
	99MTC-27	38.80	7.51	0.11701	0.511323 ± 7	89.7	523	0.4194	0.710177 ± 13	0.70931	− 24.2
	99MTC-34	37.35	7.11	0.11513	0.511458 ± 7	90.1	620	0.4608	0.710151 ± 9	0.70920	− 21.5
	99MTC-41	33.09	6.59	0.12042	0.511547 ± 9	56.0	686	0.2367	0.710151 ± 15	0.70966	− 21.9
	99MTC-42	39.27	7.90	0.12172	0.511445 ± 25	69.0	796	0.2512	0.709883 ± 14	0.70937	− 21.9
	99MTC-44	39.47	8.46	0.12959	0.511445 ± 9	44.8	675	0.1925	0.709967 ± 17	0.70957	− 22.0
	99XHL-1	34.55	6.73	0.11783	0.511548 ± 6	71.0	600	0.3431	0.709948 ± 19	0.70934	− 20.0
	99XHL-2	37.64	6.81	0.10934	0.511566 ± 10	76.8	572	0.3892	0.710004 ± 27	0.70919	− 19.3
	99XHL-4	36.52	6.47	0.10717	0.511573 ± 7	73.3	626	0.3396	0.709891 ± 15	0.70918	− 19.1
	99XHL-5	36.97	6.65	0.10872	0.511575 ± 8	75.6	625	0.3505	0.710411 ± 14	0.70968	− 19.2
	99SC-15	36.40	6.93	0.11507	0.511431 ± 8	104.9	746	0.4081	0.709379 ± 19	0.70857	− 22.1
Group 2	99XT-1	69.55	12.63	0.10986	0.511603 ± 11	117.5	1228	0.2774	0.708975 ± 15	0.70844	− 18.7
	99XT-2	71.36	12.60	0.10678	0.511601 ± 7	89.4	974	0.2660	0.708937 ± 15	0.70843	− 18.7
	99XT-3	71.93	12.69	0.10671	0.511588 ± 8	87.2	1052	0.2404	0.708759 ± 16	0.70830	− 18.9
	99XT-4	72.63	12.92	0.10757	0.511678 ± 9	75.3	980	0.2227	0.708848 ± 20	0.70842	− 17.2
	99XT-11	67.72	12.36	0.11035	0.511589 ± 7	65.4	783	0.2424	0.708820 ± 13	0.70836	− 19.0
	99XT-15	70.77	12.28	0.10497	0.511583 ± 6	102.7	1002	0.2973	0.708519 ± 17	0.70803	− 19.2
	20BHY-13	73.22	12.34	0.10192	0.511722 ± 7	78.3	1009	0.2233	0.707791 ± 20	0.70736	− 16.2
	20BHY-14	70.34	12.49	0.10744	0.511692 ± 9	78.9	955	0.2405	0.708221 ± 20	0.70776	− 16.9

$^{147}Sm/^{144}Nd$ and $^{87}Rb/^{86}Sr$ are calculated using the Sm, Nd, Rb and Sr abundances by ICP-MS. The initial isotopic ratios are respectively corrected using mean age of 140 Ma for group 1 and 130 Ma for group 2 (Wang et al., 2002).

rocks that developed very high Sr and low Nd isotopic ratios (initial $^{87}Sr/^{86}Sr = 0.7074 - 0.7084$ and $\varepsilon_{Nd}(t) = -16.2$ to -19.2), the group 1 rocks exhibit more enriched Sr and Nd isotopic signatures (initial $^{87}Sr/^{86}Sr = 0.7084 - 0.7098$ and $\varepsilon_{Nd}(t) = -24.4$ to -19.1).

5. Discussion

5.1. Effect of crustal contamination and magmatic mixing

The significant negative Nb and Ta anomalies (Fig. 4c and d) and highly enriched Sr–Nd isotopic signatures in both groups of the NHB volcanic rocks (Fig. 8) imply that crustal materials could have been significantly involved in their petrogenesis. In the group 1 rocks, however, it seems unlikely that a primitive melt was contaminated by continental upper crust with high Th concentration (e.g., 10.7 ppm, Taylor and McLennan, 1985) because of the negative anomalies of Th relative to Ba (Fig. 4c). Thus, if crustal contamination had occurred, the contaminant should be an ancient lower continental crust (LCC) component, such as the granitic gneisses of Kongling Group in the Yangtze block with time-integrated enriched Sr–Nd isotopic compositions (Gao et al., 1999; Ma et al., 2000). However, mass-balance consideration implies that the geochemical and isotopic features of the group 1 rocks could be produced by crustal contamination neither of a MORB-like nor of an enriched mantle-derived melt. For instance, if the

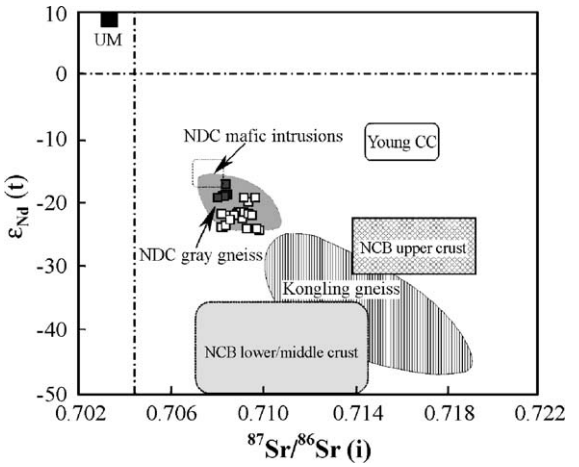

Fig. 8. $\varepsilon_{Nd}(t)$ vs. initial $^{87}Sr/^{86}Sr$ plots of the late Mesozoic rocks in NHB. Note that the two volcanic suites have similar Sr and Nd isotopic ratios to the NDC gray gneisses and are plotted between the NDC mafic intrusions and Kongling gneisses. Data sources: NDC mafic–ultramafic intrusions, NCB upper crust and Young CC (Jahn et al., 1999 and references therein); Kongling granitic gneisses (Gao et al., 1999; Ma et al., 2000); the NDC gray gneisses and granitic plutons (Xie et al., 1996; Zheng et al., 2000, Ma et al., 1998; 2000); NCB middle-lower crust (Jahn and Zhang, 1984), UM: depleted upper mantle (Sun and McDonough, 1989). Symbols as in Fig. 2.

Fig. 9. Sr–Nd isotopic modelling between different sources and/or melts. The parameters for end-member components used in this paper are:

Component	UM	Basalt	Yangtze LCC	EM	EM-derived melt
SiO_2 (wt.%)	45	52	66	47	52
$^{87}Sr/^{86}Sr(t)$	0.703	0.703	0.712	0.707	0.707
Sr [ppm]	20	150	320	48	800
Nd [ppm]	1.2	15	20	3.02	45
ε_{Nd} (t)	+8	+8	−35	−16	−16

(a) crust contamination model; (b) source contamination model. The mixing curve in (a) show that the about 50–70% and 30–60% Kongling gneiss would have been involved into depleted mantle-derived or EM-derived basalts during the group 1 melt ascent. In (b), the Sr and Nd isotopic ratios of the two volcanic suites favor source mixing between 5–20% and <5% Kongling gneiss and >80% enriched lithospheric mantle respectively for the groups 1 and 2 rocks. Data sources: UM: upper mantle (Sun and McDonough, 1989); Kongling granitic gneiss (Gao et al., 1999; Ma et al., 2000); EM denotes the enriched lithosphere mantle beneath the Dabie orogen as proposed by Jahn et al. (1999). EM-derived melt was supposed for a normal basalt corresponding to 52% in SiO_2, approximate to 20BHY-13, 20BHY-14 from the group 2 suite. Symbols as in Fig. 2.

primary melt were MORB-like, addition of 50–70% Kongling granitic gneisses would be needed to generate the observed Sr and Nd isotopic ratios in for the group 1 rocks (Fig. 9a). This could not be re-equilibrated for heat budget. Similarly, even if the primitive melt had been derived from an enriched lithospheric mantle, such as mafic intrusions reported by Jahn et al. (1999) and/or the group 2 basaltic lavas of the NHB, Sr–Nd isotopic consideration called for 30–60% of the Kongling granitic gneisses to be involved into the parental magma (Fig. 9a).

The group 2 rocks have lower $^{87}Sr/^{86}Sr$ and higher $^{143}Nd/^{144}Nd$ ratios than the group 1 lavas. They appear similar to those early Cretaceous mafic to ultramafic intrusions and basaltic lavas in the

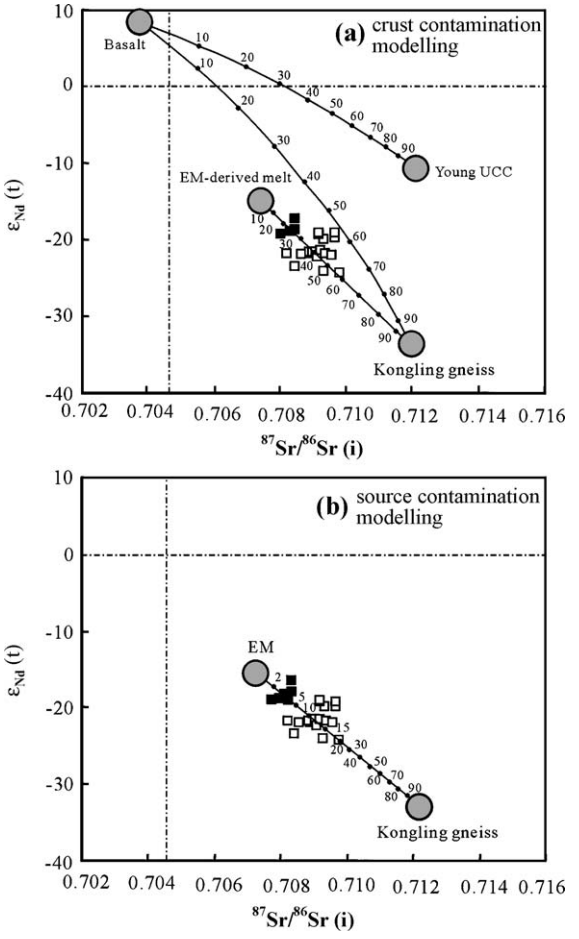

Dabie-Sulu orogenic belt (Jahn et al., 1999; Fan et al., 2001). The high Ba/Nb and La/Nb ratios in these rocks could not be attributed to crustal contamination of MORB, or of low La/Nb magmas (Fig. 7). Further, the relatively homogeneous Sr–Nd isotopic data and slightly varied K_2O/P_2O_5 (3.6–6.6) and K_2O/TiO_2 (2.0–3.6) ratios tend to indicate insignificant crustal contamination during magmatic evolution.

Alternatively, magmatic mixing between mantle- and crust-derived melts could produce the rock types of the group 1 suite. However, if magmatic mixing had occurred, the large variation in SiO_2, MgO and Sr–Nd isotopic ratios would have required for different proportion of magmatic end-members. This would certainly lead to geochemical heterogeneity in the group 1 rocks unless both end-members have similar trace element abundances. For instance, the basaltic end member such as the group 2 basaltic trachyandesite has much higher LREE (e.g., La = 87–104 ppm), TiO_2 (1.3–1.6%) and P_2O_5 (0.72–0.88%) than that of the granitic plutons (La = 12–90 ppm, TiO_2 = 0.04–0.89%, P_2O5 = 0.02–0.52%) in the Dabie Orogen (Ma et al., 1998). This means that magmatic mixing between a mantle-derived basaltic component and a crust-derived felsic melt would have generated melts with variable LREE, Ti and P contents rather than that observed in the group 1 rocks (Fig. 3). Therefore, a simple binary magma mixing model could not be a suitable interpretation for the generation of the group 1 melts. In summary, neither crust contamination nor magma mixing could account for the geochemical and isotopic signatures in both groups of the NHB volcanic rocks.

5.2. Fractional crystallization

The different eruption ages, the lack of systematic geochemical variation trend (Figs. 3, 5 and 6) and different Sr–Nd isotopic data between the groups 1 and 2 rocks (Fig. 8) suggest that the two volcanic suites were not comagmatic and could not be produced simply through FC of similar parent magmas. For the group 1 lavas, although the broad change in SiO_2 and MgO (Fig. 3), the absence of correlations between Mg#, SiO_2, Th and Ni (Fig. 4) indicate a less important role of FC en route to the surface,. as indicated from the positive correlation between La/Sm and La (Fig. 6a). Probably, their geochemical and isotopic variations were controlled by both source characteristics and different degrees of melting (Fig. 6).

In the group 2 basaltic samples, systematic variations between some major and trace elements and SiO_2 were observed, calling for crystal fractionation during magma evolution. Olivine and clinopyroxene are major fractional phases in accordance with the rapid decrease in MgO, FeOt, CaO and Ni following a SiO_2 increase (Figs. 3 and 4). Some proportion of plagioclase was also fractionated to account for the limited decreased Al_2O_3 (15.15–16.65%) and Sr (783–1405 ppm) variations (Fig. 3), as suggested by their weakly negative Eu anomalies in the chondrite-normalized REE patterns (Fig. 4b).

5.3. Source characteristics for the group 1 rocks

High-K calc-alkaline felsic rocks can be generated as results of remelting either of lower/middle continental crust, or of mixing between mantle-derived and crust-derived melts (e.g., Foley, 1992; Chalot-Prat and Boullier, 1997; Davis and von Blanckenburg, 1995; Borg and Clynne, 1999; Fan et al., 2001). The highly enriched Sr–Nd isotopic compositions in the group 1 rocks require sources with time-integrated LREE and LILE enrichment such as an ancient lower continental crust, and/or a mantle metasomatized by continental crustal melts. The possible source characteristics of the group 1 volcanic rocks will be constrained by their geochemical and isotopic signatures in the following text.

5.3.1. A pure crustal origin?

The intermediate-felsic compositions and high $^{87}Sr/^{86}Sr(i)$ ratios but low $\varepsilon_{Nd}(t)$ values in the group 1 lavas make one to speculate a pure crustal origin. In the northern Dabie orogen, the widely exposed NDC grey gneisses, which have developed very similar Sr and Nd isotopic compositions to group 1 (Xie et al., 1996; Ma et al., 2000; Zheng et al., 2000), were a likely source for these rocks. However, it has been suggested that melting of gray gneisses induced by muscovite- and biotite-dehy-

dration will generally produce potassium-rich and strongly peraluminous melts rather than the metaluminous to slightly peraluminous group 1 melts (Thompson, 1982; Patiño Dounce et al., 1990; Gardien et al., 1995). Furthermore, mass balance consideration argues against the possibility that the NDC gray gneisses with average SiO_2>62% (Zheng et al., 2000) would produce more mafic melts with SiO_2 < 62%. Consequently, the parental melts of group 1 could not be directly generated through remelting of the NDC gray gneisses.

Discovery of crustal rocks >3.2 Ga from Kongling Group in the Yangzte Block (Qiu et al., 2000) indicate the existence of an Archean lower crust rocks, which have developed extremely low ε_{Nd} (140 Ma) values (−25 to −47) and high $^{87}Sr/^{86}Sr$ (140 Ma) ratios (0.710–0.719) (Fig. 8) (Gao et al., 1999; Ma et al., 2000). Although the compositional and lithological data for the Yangtze middle-lower crust are limited, the available data seems to suggest a middle-lower crust of intermediate composition as represented by the Kongling Group (Gao et al., 1999; Ma et al., 2000). According to Gao et al. (1999), the Kongling Group is composed of dioritic–tonalitic–trondhjemitic–granitic (DTTG) rocks (50% in volume), metasedimenary rocks (45% in volume) and a small proportion (about 5% in volume) of amphibolites and mafic granulites as lens, puddings and interbeddings in the felsic gneisses. Remelting products of the Kongling DTTG gneisses will display more enriched Sr and Nd isotopic signatures than those currently observed in the group 1 rocks (ε_{Nd}(140 Ma) = −19.1 to −24.4). Yet, they could not be generated by remelting of the felsic crustal rocks beneath the North China Block (NCB) because the lower crustal rocks in the NCB have even older ages and develop more enriched Sr and Nd isotopic compositions than those from the Yangtze Block (Fig. 8) (e.g., Jahn and Zhang, 1984). Similarly, Sr–Nd isotopic comparison between the group 1 lavas and the possible mafic components (such as the Kongling amphibolites, mafic granulites and UHP eclogites, which span an $^{87}Sr/^{86}Sr$ (140 Ma) range of 0.704–0.708 and ε_{Nd} (140 Ma) range of −18 to +0.5) of the Yangtze lower-middle crust suggests that the group 1 melts can not solely originate from these mafic components.

Alternatively, melting of a source through a different proportional mixing between the amphibolites and mafic granulites and the gneisses in Kongling Group is a way to produce the group 1 magmas. If so, the voluminous felsic lavas would require tremendous heat supply provided either by basaltic underplating or crustal thickening (e.g., Patiño Dounce et al., 1990; Bergantz, 1989). Field observations reveal that there lacked contemporaneous mafic rocks in the NHB, which precludes the possibility for coeval large-scale basaltic magmatism and/or underplating episode. Additionally, experimental data from quartz-excess $CaO + MgO + Al_2O_3 + SiO_2 + H_2O$ systems under water-excess and water-deficient conditions at 10 kb showed that the produced felsic melts are peraluminous rather than metaluminous as observed in most of the group 1 rocks (Fig. 2c, Ellis and Thompson, 1986). Further, structural deformation analysis on the Dabie orogen and its surrounding areas indicated that the regional extension started from late Jurassic (e.g., Hacker et al., 2000; Wang et al., 1996). It is hence unlikely for crustal thickening to provide tremendous heat supply for large-scale crustal melting. Therefore, the group 1 rocks were unlikely to be directly generated through melting of a different proportional mixing source between the mafic and felsic rocks like those in the Kongling Group. As a whole, a pure crustal origin seems unsuitable to explain the geochemical and isotopic variations in the group 1 lavas.

5.3.2. Enriched mantle-derived melts?

Geochemical studies of the early Cretaceous mafic to ultramafic intrusions and basaltic lavas in the Dabie-Sulu belt indicated the presence of an enriched lithospheric mantle beneath the region (Jahn et al., 1999; Fan et al., 2001; Li et al., 1998). The enriched lithospheric mantle was characterized by highly enriched Sr and Nd isotopic signatures (ε_{Nd} (120 Ma) = −14 to −18, $^{87}Sr/^{86}Sr$ (120 Ma) = 0.7065–0.7080), as evidenced by the early Cretaceous mafic intrusions in the NDC. If the group 1 melts were generated directly from such an enriched lithospheric mantle, then crust contamination or AFC process should be responsible for their much higher $^{87}Sr/^{86}Sr(i)$ ratios and even lower $\varepsilon_{Nd}(t)$ values. As discussed earlier,

however, crust contamination or AFC process had played insignificant role in the evolution of the group 1 rocks. It is therefore unlikely for these rocks to be directly derived from the same enriched mantle sources as that tapped by the younger mafic rocks in the Dabie-Sulu belt (Jahn et al., 1999; Fan et al., 2001).

5.3.3. A possible source: an enriched lithosphere mantle with trapped continental crust slices

The aforementioned discussion indicates that partial melting of neither a continental middle-lower crust nor enriched lithospheric mantle sources alone could well account for the genesis of the group 1 rocks. Sr and Nd isotopic comparison among the group 1 rocks, the Kongling granitic gneisses and the early Cretaceous mafic–ultramafic intrusions in the NDC tends to suggest a hybrid source between an enriched lithospheric mantle and the continental crust.

As shown in Fig. 9b, isotopic modeling reveal that addition of 5–20% Kongling gneisses into the enriched lithosphere mantle that defined by early Cretaceous mafic–ultramafic intrusions (Jahn et al., 1999) will suffice to generate the observed Sr–Nd isotopic compositions in the group 1 rocks. Injection of 5–20% lower crust into the lithosphere mantle would not only change the Sr–Nd isotopic ratios but also the major and trace element concentrations in the source. Assuming that average SiO_2 contents in DTTG rocks is 66% (Gao et al., 1999; Ma et al., 2000), then SiO_2 contents in the mixed source spanned a range of 48–51% if the metasomatized lithospheric mantle had 47% SiO_2 (Fig. 10) as inferred by Jahn et al. (1999). Partial melting of such a mixed source in which both components were preserved in a sandwich-like structure can explain the elemental and isotopic

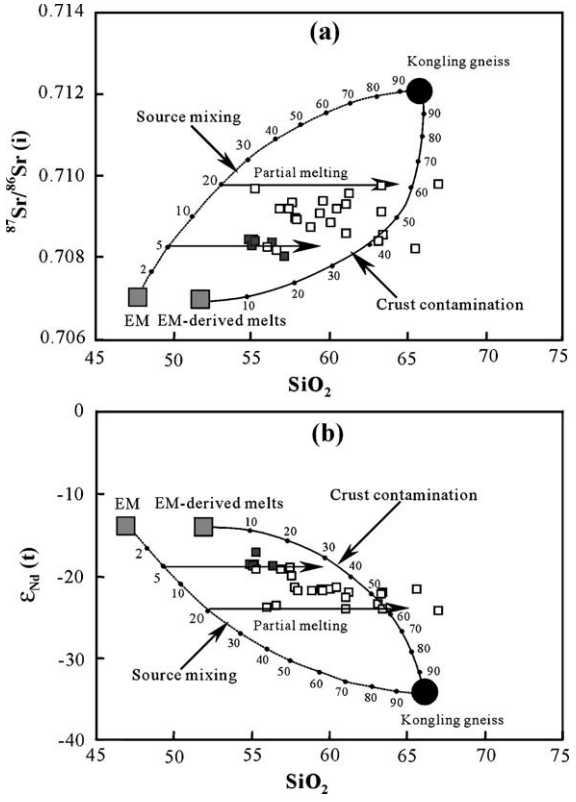

Fig. 10. SiO_2 vs. $^{87}Sr/^{86}Sr$(i) (a) and ε_{Nd}(t) (b) diagrams. The modelling results show that partial melting of a pre-existent metasomatized mantle reservoir mixed with ~5% and 5–20% lower crust can well account for the variations in SiO_2 and Sr–Nd isotopic ratios for the groups 1 and 2 rocks, respectively. The modelling parameters are the same as in Fig. 9. Symbols as in Fig. 2.

variations in the group 1 rocks (Figs. 3, 4 and 8). For instance, sample 99XT-6 have the highest SiO_2, and also the highest $^{87}Sr/^{86}Sr$(i) and lowest ε_{Nd}(t) in the group 1 suite, its source should involve the highest proportion of Kongling gneisses (about 20%) and therefore have higher incompati-

Fig. 11. A cartoon showing the formation of the sandwich-like heterogeneous mantle source and its role in the tectono-magmatic evolution of the Dabie orogenic belt. (A) About 240 Ma (e.g., Li et al., 1993; Zheng et al., 2002), the subduction and collision between the North China and Yangtze Blocks. (B) 220–180 Ma, some volume of the subducted lower crust was mechanically entrained into the lithospheric mantle during the rapid exhumation of the HP–UHP rocks from the mantle depths to middle-lower crust as a consequence of slab break-off (e.g., Andersen et al., 1991; Faure et al., 1999; Li et al., 1999; Xu et al., 1999). (C) 150–136 Ma, convective thinning and unrooting of the thickened lithosphere led to the extensional tectonics (e.g., Hacker et al., 2000) and widespread melting of the sandwich-like heterogeneous mantle source to produce the melts for the group 1 rocks. (D) 132–116 Ma, lithospheric thinning continued to trigger the melting of the source with less volume of subducted middle-lower crust slices, generating the melts for the group 2 rocks.

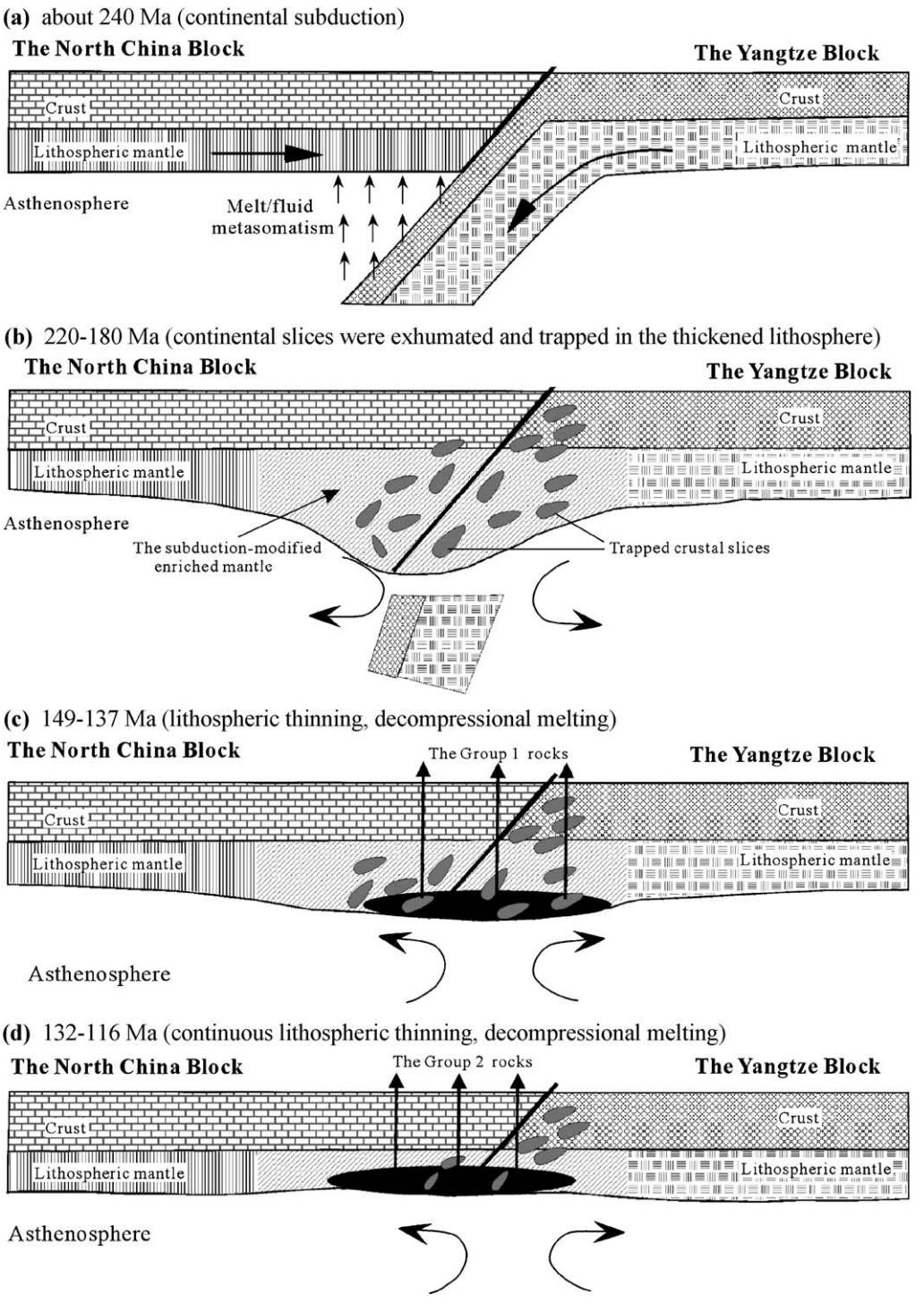
(a) about 240 Ma (continental subduction)
The North China Block
The Yangtze Block
Crust
Lithospheric mantle
Crust
Lithospheric mantle
Asthenosphere
Melt/fluid metasomatism
(b) 220-180 Ma (continental slices were exhumated and trapped in the thickened lithosphere)
The North China Block
The Yangtze Block
Crust
Lithospheric mantle
Crust
Lithospheric mantle
Asthenosphere
The subduction-modified enriched mantle
Trapped crustal slices
(c) 149-137 Ma (lithospheric thinning, decompressional melting)
The North China Block
The Group 1 rocks
The Yangtze Block
Crust
Lithospheric mantle
Crust
Lithospheric mantle
Asthenosphere
(d) 132-116 Ma (continuous lithospheric thinning, decompressional melting)
The North China Block
The Group 2 rocks
The Yangtze Block
Crust
Lithospheric mantle
Crust
Lithospheric mantle
Asthenosphere

ble trace element contents than others. In contrast, for those samples from Xianhualing area (e.g., 99XHL-1) with relatively lower SiO_2 contents and less enriched Sr–Nd isotopic signatures, addition of only 5% Kongling gneisses in the enriched lithospheric mantle can explain their geochemical and isotopic features. Source heterogeneity by mixing in different proportions between the lower continental crust and the enriched lithospheric mantle, incorporating with different partial degrees of partial melting, therefore, may well interpret the geochemical characteristics in the late Mesozoic group 1 volcanic rocks.

5.4. Source characteristics of the group 2 rocks

Recent studies (e.g., Jahn et al., 1999; Fan et al., 2001; Li et al., 1998) demonstrated that the early Cretaceous mafic–ultramafic rocks and basaltic lavas in the Dabie-Sulu orogenic belt were generated from partial melting of metasomatized lithospheric mantle or metasomatized mantle wedge. The group 2 rocks are contemporaneous in eruption age and share similar geochemical characteristics to the mafic–ultramafic intrusions in the Dabie belt and basaltic lavas along the Sulu belt (Jahn et al., 1999; Fan et al., 2001). Their slightly more enriched Sr–Nd isotopic signatures could be a result of either crust contamination or a few percent of middle-lower crust slices trapped in the melting source or heterogeneity of the enriched lithospheric mantle reservoir. As illustrated in Figs. 9 and 10, chemical and isotopic modelling results show that either partial melting of a sandwich source with $<5\%$ Kongling granitic gneisses in the enriched lithospheric mantle or addition of 15–30% lower crust materials to EM-derived melts en route to the surface can account for their geochemical and isotopic features. Considering the limited variations in Sr–Nd isotopes and in K_2O/P_2O_5 (3.6–6.6) and K_2O/TiO_2 (2.0–3.6) ratios in the group 2 rocks, it is reasonable to conclude that a sandwichlike source rather than crustal contamination en route to the surface should contribute to their petrogenesis.

Relative to the group 1 lavas, the group 2 rocks have high LILE, LREE and HFSE concentrations (Fig. 3), indicating their generation from lower degrees of partial melting. The source contained less volume of the trapped lower crust slices as suggested by their less enriched Sr–Nd isotopic compositions. Collectively, it appears likely that the contribution of subducted continental crustal slices trapped in the lithospheric mantle had been progressively reduced from the groups 1 to 2 NHB rocks following the thinning and extensional process of the thickened lithosphere (Fig. 11).

5.5. Implications for the tectonic evolution in the Dabie collisional belt

It is widely accepted that the collision between the Yangtze and North China Blocks occurred at ca. 240 Ma and the first stage for the exhumation of the HP-UHP rocks in Dabie-Sulu belt took place at 226–214 Ma (e.g., Li et al., 1993, 1999; Zheng et al., 2002 and references therein). As discussed earlier, the geochemical and isotopic signatures of the both suites of late Mesozoic NHB volcanic rocks suggest a sandwich-like source composed of an enriched lithospheric mantle and the subducted continental middle-lower crust slices. The time interval between the collision/early exhumation event ($\sim$ 240 Ma) and the NHB volcanism (149–116 Ma) indicate that the trapped subducted crust slices had been preserved in the lithospheric mantle for tens of million years. The arising questions are: (1) how these crustal materials were mixed in the mantle? (2) Under which conditions could they be preserved for such a long time? and (3) what role had they played in the tectonic evolution of the collisional orogenic belt?

The wide spectrum of the HP-UHP rocks in the Dabie-Sulu belt suggest that the continental middle-lower crust were entirely subducted to mantle depths (e.g., Xu et al., 1992; Cong, 1996; Ye et al., 2000; Zheng et al., 2002). According to Andersen et al. (1991) and Faure et al. (1999), significant volume of subducted crustal materials could be settled in upper mantle during the deep continental subduction and subsequent exhumation of the HP-UHP rocks in response to the buoyancy from the convective mantle. Unlike the tectonic models proposed by Jahn et al. (1999) and Li et al. (1998), which proposed that the subducted crustal materials were either bulk mixed with the upper mantle

peridotites or dehydrated to release fluids to metasomatize the mantle wedge, we propose that the trapped subducted continental middle-lower crust slices inferred by the late Mesozoic NHB volcanic rocks appears to be mechanically and tectonically entrained in the enriched lithospheric mantle following the continental subduction and exhumation of the HP-UHP rocks.

Undoubtedly, these crustal materials could not be preserved for a long time as an underplating layer at the base of the thickened lithosphere, at which they would be decomposed or melted due to the potential temperature of convective mantle (e.g., Olafsson and Eggler, 1983). Most probably, they were trapped into the lithospheric mantle, which was formed during slab subduction before ~240 Ma (Fig. 11A), in forms of puddings and lens or as interbeddings and preserved in a sandwich-like structure (Fig. 11B). At the beginning of late Jurassic (about 150 Ma), extensive tectonic extension and thermal doming incorporating with eastward lateral escape resulted in a rapid lithospheric unrooting event and further exhumation of the HP-UHP rocks in Dabie-Sulu belt (Li et al., 1999; Jahn et al., 1999; Hacker et al., 2000; Fan et al., 2001). In comparison with the enriched lithospheric mantle beneath the Dabie-Sulu belt, the trapped lower continental crust acted as the most fertile component with low melting temperature. These crustal materials are sensitive to thermal perturbation induced by lithospheric extension. The heterogeneous source trapping more lower continental crust materials was melted firstly to generate the group 1 melts (Fig. 10C). As partial melting continued, the source containing less crustal slices melted, producing melts for the group 2 rocks (Fig. 11D). The formation of the sandwich-like heterogeneous source and its role in the tectonic evolution of the Dabie orogenic belt are summarized as Fig. 11.

6. Concluding remarks

Late Mesozoic volcanism occurring in the northern Huaiyang belt, Dabie Orogenic Belt, central China, can be grouped into two volcanic suites: the group 1 suites with eruption age of 149–137 and 132–116 Ma for the group 2 suite. Both groups of rocks show high-K calc-alkaline to shoshonitic affinities with time-integrated geochemical variations. Relative to the basaltic group 2 rocks, the felsic group 1 rocks have low MgO, FeOT, TiO_2, P_2O_5, Cr, Ni, HFSE, Sr and LREE fractionations and more enriched Sr and Nd isotopic signatures (the initial $^{87}Sr/^{86}Sr = 0.7084–0.7098$ and $\varepsilon_{Nd}(t) = -19.1$ to -24.4); the group 2 rocks are similar to the coeval mafic–ultramafic intrusions in the Dabie orogenic belt (Jahn et al., 1999).

Combined major, trace element and Sr–Nd isotopic compositions of the two volcanic suites in the NHB suggest their derivation from a mixed source between the enriched lithospheric mantle and the subducted continental lower-middle crust of the Yangtze Block. Melting of the mixed source containing higher proportion of crustal materials produced the earlier group 1 intermediate-felsic rocks, and lower proportion of these materials for generation of the younger group 2 basaltic melts. The petrogenesis of the late Mesozoic volcanism in the NHB appears to support a sandwich-like structure of the lithospheric mantle beneath the Dabie orogenic belt, in which the subducted lower continental crust was mechanically entrained during the continental collision and subsequent exhumation of the HP-UHP rocks.

Acknowledgements

The authors would like to thank Mr. L. Qi for his help in ICP-MS performance and Mr. R.F. Zhang for Sr–Nd isotope analysis. Dr. F. Chalot-Prat, Prof. C.Q. Ma and Prof. R.L. Rudnick are appreciated for their thoughtful and constructive comments and reviews, which significantly improved the early version of the manuscript. This work was financially supported by Chinese National Natural Science Foundation (49873011 and 40073011), Ministry of Science and Technology, China (G1999075504) and Chinese Academy of Sciences (KZCX1-105). **[RR]**

Appendix

The XRF analytical results of international standards

Standard	GSR-1 (granite)		GSR-2 (andesite)		GSR-3 (basalt)	
	This work, n=4	Reference	This work, n=10	Reference	This work, n=6	Reference
SiO_2	72.48±0.13	72.83	61.20±0.13	60.62	45.10±0.09	44.64
Al_2O_3	13.46±0.09	13.40	16.31±0.13	16.17	14.21±0.14	13.83
TFe_2O_3	2.25±0.10	2.14	4.38±0.06	4.90	13.23±0.18	13.40
FeO	1.00		2.32		7.43	
MgO	0.39±0.07	0.42	1.68±0.08	1.72	7.73±0.18	7.77
CaO	1.72±0.05	1.55	5.31±0.09	5.20	8.76±0.10	8.81
Na_2O	3.10±0.05	3.13	3.74±0.13	3.86	3.47±0.10	3.38
K_2O	4.97±0.12	5.01	1.81±0.05	1.89	2.41±0.11	2.32
TiO_2	0.30±0.05	0.29	0.51±0.01	0.52	2.35±0.05	2.36
MnO	587±35 ppm	598 ppm	801±20 ppm	780 ppm	1672±72 ppm	1690 ppm
P_2O_5	903±24 ppm	928 ppm	2290±15 ppm	2360 ppm	9450±62 ppm	9462 ppm
LOI (900 °C)		0.69		4.44		2.24
H_2O^+	0.59		1.58		2.68	
CO_2	0.17		3.39		0.19	
Total	99.59	99.613	99.96	99.64	100.46	99.87

References

Ames, L., Tilon, G.R., Zhou, G., 1993. Timing of collision of the Sino-Korean and Yangtze Cratons: U–Pb zircon dating of coesite-bearing eclogites. Geology 21, 339–342.

Ames, L., Zhou, G., Xiong, B., 1996. Geochronology and isotopic character of highpressure metamorphism with implications for collision of the Sino-Korean and Yangtze Cratons, central China. Tectonics 15, 472–489.

Andersen, T.B., Jamtveit, B., Dewey, J.F., Swensson, E., 1991. Subduction and eduction of continental crust: major mechanism during continent–continent collision and orogenic extensional collapse, a model based on the south Norwegian Caledonides. Terra Nova 3, 301–310.

Bergantz, W.V., 1989. Underplating and partial melting: implications for melt generation and extraction. Science 245, 1093–1095.

Borg, L.E., Clynne, M.A., 1999. The petrogenesis of felsic calc-alkaline magmas from the southernmost Cascades, California: origin by partial melting of basaltic lower crust. J. Petrol. 39, 1197–1222.

Chalot-Prat, F., Boullier, A.M., 1997. Metasomatism in the subcontinental mantle beneath the Eastern Carpathians (Romania): new evidence from trace element geochemistry. Contrib. Mineral. Petrol. 129, 284–307.

Cong, B.L., (ed.), 1996. Ultrahigh-pressure metamorphic rocks in the Dabie-Sulu region of China. Science Press. Beijing: China and Kluwer Acad. Pub., Dordrecht, pp. 224.

Cong, B.L., Wang, Q.C., Zhang, H.Z., Yan, X., Jiang, L.L., 1996. Petrogenesis of Cenozoic volcanic rocks in Hefei basin, China. Acta Petrol. Sinica 12, 370–381 (in Chinese with English abstract).

Davis, J.H., von Blanckenburg, F., 1995. Slab breakoff: a model of lithosphere detachment and its test in the magmatism and deformation of collisional orogens. Earth Planet. Sci. Lett. 129, 327–343.

Eide, E.A., McWilliams, M.O., Liou, J.G., 1994. $^{40}Ar/^{39}Ar$ geochronology and exhumation of high-pressure to ultrahigh-pressure metamorphic rocks in east-central China. Geology 22, 601–604.

Ellis, D.J., Thompson, A.B., 1986. Subsolidus and partial melting reactions in the quartz excess $CaO+MgO+Al_2O_3+SiO_2+H_2O$ system under water-excess and water-deficient conditions to 10 kb: some implications for the origin of peraluminous melts from mafic rocks. J. Petrol. 27, 91–121.

Ernst, W.G., Liou, J.G., 1995. Contrasting plate-tectonic styles of the Qingling-Dabie-Sulu and Franciscan metamorphic belts. Geology 23, 353–356.

Fan, W.M., Guo, F., Wang, Y.J., Lin, G., 2001. Post-orogenic bimodal volcanism along Sulu orogenic belt in eastern China. Phys. Chem. Earth, A 26, 733–746.

Faure, M., Lin, W., Shu, L.S., Sun, Y., Scharer, U., 1999. Tectonics of the Dabieshan (eastern China) and possible exhumation mechanism of ultra high-pressure rocks. Terra Nova 11, 251–258.

Foley, S.F., 1992. Petrological characterization of the source components of potassic magmas: geochemical and experimental constraints. Lithos 28, 187–204.

Gao, S., Ling, W.L., Qiu, Y.M., Zhou, L., Hartman, G., Simon, K., 1999. Contrasting geochemical and Sm–Nd isotopic compositions of Archean metasediments from the Kongling high-grade terrain of the Yangtze Craton: evidence for cratonic evolution and redistribution of REE during crustal anatexis. Geochim. Cosmochim. Acta 63, 2071–2088.

Gardien, V., Thompson, A.B., Grujic, D., Ulmer, P., 1995. Experimental melting of biotite + plagioclase + quartz muscovite assemblages and implications for crustal melting. J. Geophys. Res. 100, 15581–15591.

Hacker, B.R., Ratschbacher, L.W., Dong, S., 1995. What brought them up? Exhumation of the Dabie Shan ultrahigh-pressure rocks. Geology 23, 743–746.

Hacker, B.R., Ratschbacher, L.W., Ireland, L., Walker, D., Dong, S., 1998. U/Pb zircon ages constrain the architecture of the ultrahigh-pressure Qinling-Dabie Orogen, China. Earth Planet. Sci. Lett. 161, 215–230.

Hacker, B.R., Ratschbacher, L., Webb, L., McWilliams, M.O., Ireland, T., Calvert, A., Dong, S.W., Wenk, H.R., Chateigner, D., 2000. Exhumation of ultrahigh-pressure continental crust in east central China: late Triassic–early Jurassic tectonic unroofing. J. Geophys. Res. 105 (B6), 13339–13364.

Jahn, B.M., Zhang, Z.Q., 1984. Archean granulite gneisses from eastern Hebei Province, China: rare earth geochemistry and tectonic implications. Contrib. Mineral. Petrol. 85, 224–243.

Jahn, B.M., Wu, F.Y., Lo, C.H., Tsai, C.H., 1999. Crust–mantle interaction induced by deep subduction of the continental crust: Geochemical and Sr–Nd isotopic evidence from post-collisional mafic–ultramafic intrusions of the northern Dabie complex, central China. Chem. Geol. 157, 119–146.

Li, Z.X., 1994. Collision between the North and South China Blocks: a crustal-detachment model for suturing in the region east of the Tanlu Fault. Geology 22, 739–742.

Li, S.G., Xiao, Y.L., Liou, D.L., Chen, Y.Z., Ge, N.J., Zhang, Z.Q., Sun, S.S., Cong, B.L., Zhang, R.Y., Hart, S.R., Wang, S.S., 1993. Collision of the North China and Yangtze blocks and formation of coesite-bearing eclogites: timing and process. Chem. Geol. 109, 89–111.

Li, S.G., Nie, Y.H., Jagoutz, E., Xiao, Y.L., Zheng, Y.F., 1997. Geochemical evidence for the recycling of subducted continental crust from Dabie Orogen, eastern China. Sci. China, Ser. D 27, 412–418.

Li, S., Nie, Y.H., Hart, S.R., Zheng, S.G., 1998. Upper mantle-deep subducted continental crust interaction: Sr and Nd isotopic constraints on the syn-collisional mafic to ultramafic intrusions in the northern Dabieshan, China. Sci. China, Ser. D 28, 18–22.

Li, S.G., Jagoutz, E., Lo, C.-H., Chen, Y.Z., Li, Q.L., 1999. Sm/Nd, Rb/Sr and $^{40}Ar/^{39}Ar$ isotopic systematics of the ultrahigh-pressure metamorphic rocks in the Dabie-Sulu belt central China: a retrospective view. Int. Geol. Rev. 41, 1114–1124.

Ma, C.Q., Li, Z.C., Ehlers, C., Yang, K.G., Wang, R.J., 1998. A post-collisional magmatic plumbing system: Mesozoic granitoid plutons from the Dabieshan high-pressure and ultrahigh-pressure metamorphic zone, east-central China. Lithos 45, 431–456.

Ma, C.Q., Ehlers, C., Xu, C.H., Li, Z.C., Yang, K.G., 2000. The roots of the Dabieshan ultrahigh-pressure metamorphic terrane: constraints from geochemistry and Nd–Sr isotope systematics. Precambrian Res. 102, 279–301.

Maniar, P.D., Piccoli, P.M., 1989. Tectonic discrimination of granitoids. Geol. Soc. Amer. Bull. 101, 615–643.

Mattauer, M., Matte, P., Malavieille, J., Tapponnier, P., Maluski, H., Xu, Z.Q., Luy, L., Tang, Y.Q., 1985. Tectonics of the Qinling belt: build-up and evolution of eastern Asia. Nature 317, 496–500.

Middlemost, E.A.K., 1994. Naming materials in the magma/igneous rock system. Earth-Sci. Rev. 37, 215–224.

Okay, A.I., Sengör, A.M.C., Satir, M., 1993. Tectonics of an ultrahigh-pressure metamorphic terrane: the Dabie Shan/Tongbai Shan orogen, China. Tectonics 12, 1320–1334.

Olafsson, M., Eggler, D.H., 1983. Phase relation of amphibole, amphibole-carbonate and phlogophite-carbonate peridotite: petrologic constraint on the asthenosphere. Earth Planet. Sci. Let. 64, 305–315.

Patiño Dounce, A.E., Humphreys, E.D., Johnston, A.D., 1990. Anatexis and metamorphism in tectonically thickened continental crust exemplified by the Sevier hinterland, western North America. Earth Planet. Sci. Let. 97, 290–315.

Qi, L., Hu, J., Gregoire, D.C., 2000. Determination of trace elements in granites by inductively coupled plasma mass spectrometry. Talanta 51, 507–513.

Qiu, Y.M., Gao, S., McNaughton, N.J., Groves, D.I., Ling, W.L., 2000. First evidence of >3.2 Ga continental crust in the Yangtze Craton of south China and its implications for Archean crustal evolution and Phanerozoic tectonics. Geology 28, 11–14.

Ratschbacher, L., Hacker, B.R., Webb, L., McWilliams, M.O., Ireland, T., Calvert, A., Dong, S.W., Chateigner, D., Wenk, H.R., 2000. Exhumation of ultrahigh-pressure continental crust in east central China: cretaceous and cenozoic unroofing and Tan-Lu fault. J. Geophys. Res. 105 (B6), 13303–13338.

Rowley, D.B., Xue, F., Tucker, R.D., Peng, Z.C., Baker, J., Davis, A., 1997. Ages of ultrahigh pressure metamorphism and protolith orthogneisses from the eastern Dabie Shan: U/Pb zircon geochronology. Earth Planet. Sci. Let. 151, 191–203.

Sun, S.S., McDonough, W.F., 1989. Chemical and isotopic systematics of oceanic basalts: implication for mantle composition and processes. In: Sauders, A.D., Norry, M.J. (Eds.), Magmatism in the Ocean Basins. Geol. Soc. Spec. Pub., vol. 42, pp. 313–345.

Taylor, S.R., McLennan, S.M., 1985. The continental crust: its composition and evolution. Blackwell, Oxford Press, p. 312.

Thompson, A.B., 1982. Dehydration melting of pelitic rocks and the generation of H_2O undersaturated granitic liquids. Am. J. Sci. 282, 1567–1595.

Wang, Q.C., Zhai, M.G., Cong, B.L., 1996. Regional geology. In: Cong, B.L., (ed), Ultrahigh-pressure metamorphic rocks in the Dabieshan-Sulu region of China. Science Press, Beijing and Kluwer Acad. Pub., Dordrecht, pp. 8–26.

Wang, Y.J., Fan, W.M. and Guo, F., 2002. K–Ar dating of Late Mesozoic volcanism and geochemistry of volcanic gravels in the North Huaiyang belt, Dabie orogen: constrains on the stratigraphic framework and exhumation of the northern Dabie orthogneiss complex.

Xie, Z., Chen, J.F., Zhou, T.X., Zhang, X., 1996. Nd isotopic compositions of metamorphic and granitic rocks from Dabie orogen and their geological significance. Acta Petrol. Sinica 12, 401–408 (in Chinese with English abstract).

Xu, S., Okay, A.I., Sengor, A.M.C., Su, W., Liu, Y., Jiang, L., 1992. Diamond from Dabie Shan eclogites and its implication for tectonic setting. Science 256, 80–82.

Xu, P.F., Sun, R.M., Liu, F.T., Wang, Q.C., Cong, B.L., 1999. The subduction and slab breakoff between the South China Block

and North China Block: evidence from the seismological chromatography. Chin. Sci. Bull. 44, 1658–1661.

Xue, F., Rowley, D.B., Tucker, R.D., Peng, Z.X., 1997. U–Pb zircon ages of granitoid rocks in the North Dabie complex, eastern Dabieshan, China. J. Geol. 105, 744–753.

Yang, Z.L., Shen, W.Z., Shen, J.L., Tao, K.Y., Xie, F.G., 1999. Isotopic geochronology of the Xianghongdian alkaline complex, northern margin of the Dabie Mountains, China. Acta Geol. Sinica 73, 1–10 (in Chinese with English abstract).

Ye, K., Ye, D.N., Cong, B.L., 2000. The possible subduction of continental material to depths greater than 200 km. Nature 407, 734–736.

Zheng, X.S., Jin, C.W., Zhai, M.G., Shi, Y.H., 2000. Approach to the source of the gray gneisses in north Dabie terrain: Sr and Nd isochron age and isotope compositions. Acta Petrol. Sinica 16, 194–198 (in Chinese with English abstract).

Zheng, Y.F., Wang, Z.R., Li, S.G., Zhao, Z.F., 2002. Oxygen isotope equilibrium between eclogite minerals and its constraints on mineral Sm–Nd chronometer. Geochim. Cosmochim. Acta 66, 625–634.

Zhou, T.X., Chen, J.F., Zhang, X., 1995. Geochemical study of the granite-syenite belt in the North Huaiyang region and its tectonic significance. Geol. Rev. 41, 144–151 (in Chinese with English abstract).